EXPERIMENTAL STUDY ON THE ELECTROHYDRODYNAMIC INSTABILITY BETWEEN TWO IMMISCIBLE LIQUIDS FLOWING IN A MICROCHANNEL

by

Sercan Altundemir

B.S., Chemical Engineering, Boğaziçi University, 2015

Submitted to the Institute for Graduate Studies in
Science and Engineering in partial fulfillment of
the requirements for the degree of
Master of Science

Graduate Program in Chemical Engineering

Boğaziçi University

2017

ACKNOWLEDGEMENTS

First of all, I would like to express my sincere gratitude to my thesis supervisor Assoc. Prof. A. Kerem Uguz for his motivation, guidance and support. It was a great experience to work with him beacuse I have learned a lot from his knowledge, expertise and wisdom in microfluidics.

I wish to express my sincere appreciations for the members of thesis committee, Prof. Ramazan yıldırım and Asst. Prof. Emrah Nikerel, for accepting to be a member of the thesis committee, devoting their valuable time to read and comment on my thesis.

I would like to thank Pınar Eribol for her instructions and assistance from the beginning of my work. Also very special thanks for Suat Canberk Ozan for his great help whenever I needed it.

I also wish to express my gratitude to Seymen İlke Kaykanat, Berkay Keklik and the members of KB 406.

I also thank my friends Ayşe Eren, Ahmet Hallaçeli, Ece Çiğdem Mutlu, Cihat Öztepe Gözde Öztürk, Ayça Soylu for their frienships through my M.Sc. years.

Cordial thanks for Bilgi Dedeoğlu, Yakup Bal, Murat Düzgünoğlu, Melike Gürbüz and Başak Ünen for their technical assistance and help.

Finally, I wish to thank my family.

Financial support for this study was provided by TÜBİTAK through project 116M374 and Boğaziçi University Research Fund Project 11521.

ABSTRACT

EXPERIMENTAL STUDY ON THE ELECTROHYDRODYNAMIC INSTABILITY BETWEEN TWO IMMISCIBLE LIQUIDS FLOWING IN A MICROCHANNEL

The aim of this study is to investigate experimentally the electrohydrodynamic instability between two Newtonian immiscible liquids in a microchannel. When two immiscible liquids flow in laminar regime, a flat interface is formed between them. If an electric field is applied on the system, the interface may deform, i.e. may become unstable. This instability, called electrohydrodynamic instability (EHD) is used for forming mono dispersed droplets. In this study, the fabrication methods of microchannels with electrodes are investigated. A microchannel of depth 350 μm, width 1.1 mm, electrode length 10 mm, and total length 20 mm, with double sided conductive and non-conductive tape on PMMA is fabricated. Silicone oil with different viscosities and ethylene glycol are injected into the channel via a syringe pump and a DC electric field in the range of 200-1600 V is applied normal to the flow direction. The effect of the parameters such as the flow rate ratio, depth ratio, viscosity ratio and the total flow rate of the liquid couple, on the critical voltage at which the interface starts to destabilize is investigated. Then the effect of total flow rate on the time elapsed for the interface to be ruptured to form droplets by hitting the wall of the channel is analyzed. Finally, the effect of each parameter on the size of droplets at various voltages is investigated. It is observed that an increase in the viscosity or the flow rate ratio of the silicone oil to the ethylene glycol has a stabilizing effect, i.e. a higher voltage is needed while the total flow rate has no effect on it. However, it is observed that an increase in the total flow rate results in shortening of the elapsed time for the interface to hit the wall. Moreover, the droplet size decreases down to 0.1 μL with an increase in the applied voltage, the viscosity ratio or the total flow rate or a decrease in the flow rate ratio. In addition to these observations, two empirical models for determining the critical electric number, i.e., the dimensionless voltage and the droplet size and another model which is a combination of both models, for determining the droplet size at the critical voltage are established.

ÖZET

BİR MİKROKANALDA AKAN BİRBİRİNE KARIŞAMAYAN İKİ SIVI ARASINDAKİ ELEKTROHİDRODİNAMİK DENGESİZLİK ÜZERİNE DENEYSEL ÇALIŞMA

Bu çalışmanın amacı birbirine karışamayan Newtonyen iki sıvı arasındaki elektrohidrodinamik dengesizliği deneysel olarak incelemektir. İki birbirine karışmayan sıvı laminar rejimde akarken; aralarında düz bir arayüzey oluşur. Eğer sisteme elektrik alan uygulanırsa, arayüzey biçimsizleşebilir, başka bir deyişle kararsız hale gelebilir. Elektrohidrodinamik dengesizlik olarak adlandırılan, arayüzeydeki bu kararsızlık mikro damlacık oluşturmak için kullanılır. Bu çalışmada, elektrotlu mikrokanal üretim yöntemleri tartışıldı. PMMA üzerine çift taraflı iletken bant ve iletken olmayan tek taraflı bantla; 350 μm derinliğinde, 1.1 mm genişliğinde, elektrot uzunluğu 10 mm'lik ve toplam uzunluğu 20 mm'lik bir mikrokanal üretildi. Farklı viskozitelerde silikon yağı ve etilen glikol şırınga pompası yardımıyla kanalın içine enjekte edildi ve 200 ile 1600 V aralığında bir DC elektrik alanı akış yönüne dik olarak uygulandı. Sıvı çifitinin toplam debi, viskozite oranı ve debilerinin oranı gibi parametrelerin, arayüzeyin dengesizleşmeye başladığı kritik voltaj üzerindeki etkisi incelendi. Sonra toplam debinin, arayüzeyin damlacık oluşturmak üzere bozulması için geçen zamanın üzerindeki etkisi analiz edildi. Son olarak, her parametrenin çeşitli voltajlardaki damlacık boyutu üzerine olan etkisi incelendi. Toplam debinin kritik voltaj üzerinde hiç bir etkisi yokken, silikon yağının etilen glikole göre olan viskozite veya debilerinin oranındaki artışın, arayüzey üzerinde kararlaştırıcı bir etkisi olduğu gözlemlendi. Başka bir deyişle, kararsızlık için daha yüksek bir voltaja ihtiyaç duyuldu. Bununla beraber, toplam debinin artışının, arayüzeyin duvara çarpma süresini kısalttığı ve damlacık boyutunu küçülttüğü gözlemlendi. Ayrıca, damlacık boyutları, uygulanan voltajdaki, viskozite oranındaki veya toplam debideki bir artma ile ya da debilerinin oranındaki bir azalma ile 0.1 μL'ye kadar küçülmektedir. Bu gözlemlere ek olarak, kritik elektrik sayısının ve damlacık boyutunun hesaplanması için iki tane ve kritik voltajdaki damlacık boyutunun hesaplanması için de bu iki modelin birleşmesi olan bir tane deneysel model kuruldu.

TABLE OF CONTENTS

LIST OF FIGURES

LIST OF TABLES

LIST OF SYMBOLS

d_i	Thickness of the liquid i
E_b	Electrical Number
$H^{(i)}$	Depth of liquid i
H_r	Depth ratio
Q_r	Flow rate ratio
$Q^{(i)}$	Flow rate of liquid i
V	Voltage
W	Width
γ	Interfacial tension
$\boldsymbol{\varepsilon}$	Electrical permittivity
μ	Viscosity
$\mu^{(i)}$	Viscosity of liquid i
μ_r	Viscosity ratio
ν	Kinematic viscosity
ρ	Density
σ	Electrical conductivity

LIST OF ACRONYMS/ABBREVIATIONS

2D	Two-dimensional
3D	Three-dimensional
AC	Alternative Current
C	Critical
CNC	Computer numerical control
DC	Direct Current
EHD	Electrohydrodynamic
EK	Elektrokinetik
FOV	Field of view
PC	Polycarbonate
PDMS	Polydimethylsiloxane
Pé	Péclet number
PMMA	Poly(methyl methaaccrylate)
PS	Polystyrene
PVC	Polyvinylchloride
Re	Reynolds number
TPE	Thermoset polyester
UV	Ultraviolet

1. INTRODUCTION

Microfluidics is a science studying the behavior of fluids in micro-sized systems consisting of micro structures such as channels, wells and chambers which may serve functions in sensing mechanism, reaction or fluid control (e.g. separation, mixing, filtering, pumping, valving (Fiorini and Chiu, 2005)). Microfluidics can also be defined as a technology allowing many large-scale laboratory applications to be miniaturized on a single device called lab-on-a-chip and integrated to each other. The microfluidic systems can be employed for chemical or biological analysis and measurement; e.g. analyte concentration (Kamholz *et al.*, 1999), viscosity (Jun Kang *et al.*, 2013), pH (Magnusson *et al.*, 2013), fluid density (Sparks *et al.*, no date), chemical (Bulutoglu *et al.*, 2016) or biological (Seo *et al.*, 2012) reaction, droplet formation (Nisisako *et al.*, 2002), cell culturing (Hsiao *et al.*, 2009), immunoassay (Xiang *et al.*, 2014) and polymerase chain reaction (Lagally *et al.*, 2000). The microfluidic systems have a very significant role on today's developing technology and still continue to lift its effectiveness in many fields starting from its first use in small tubes carrying ink for printing in 1950s (Slapar, 2008). Microfluidic systems offer many advantages such as the use of small sample size, affordability, rapid analysis, portability, better sensitivity and no need for complex equipment and laboratory (Whitesides, 2006).

The microfluidic devices since 1980s, where the microfluidics era began, have been fabricated by several methods and from several materials; e.g. elastomers, thermosets, thermoplastics, hydrogels, paper, and hybrid and composite materials (Ren *et al.*, 2013). The first microfluidic devices were fabricated from silica or glass due to the advantages of good chemical and physical stability, good optical properties such as light transmittance and compatibility with solvents (Zhou *et al.*, 2010). In the early stages of microfluidic devices, silicon micro-machining technique, which was previously used in the fabrication of microelectromechanical systems (MEMS), has been employed (Fong Lei, 2015). Moreover, etching and photolithography have become the most preferred technique for glass and silica. However, the fabrication of glass or silica based microfluidic chips are slow and it requires facilities like clean room and manpower. Therefore, less expensive and nonfragile materials such as polymers and plastics were then considered (Zhou *et al.*, 2010). For thermoplastics and polymers, the hot embossing and imprinting techniques (mostly the silicon stamp as the

imprinting tool) were employed (Becker and Locascio, 2002). Almost a decade ago, paper has been employed for the first time as the material since polymers have still the disadvantages of incompatibility with solvents, irresistibility to heat. Paper is biocompatible, lightweight, cheap and fabrication methods were easy, low-cost and allow high throughput production (Atalay *et al.*, 2011).

In microchannels, the flow is usually laminar since the Reynolds (Re) number, which shows the ratio of inertial to viscous forces is very low (Re < 1) (Atencia and Beebe, 2005). Moreover, the fluid transport is induced by the bulk motion of the fluid in a microchannel since the Péclet number is usually high (Pé>1), which means that the effect of mass convection is higher than that of mass diffusion. Therefore, the liquids don't show turbulent behavior and doesn't get mixed easily. For two miscible liquids flowing parallel to each other in a microchannel, mixing becomes a problem because of the non-applicability of the conventional methods of larger scales (Schwesinger *et al*., 1996). In order to solve this problem, novel strategies based on inducing instability on the interface between those liquids were proposed (Hosokawa *et al*., 1999). A similar instability mechanism is also proposed when two immiscible liquids share a common interface in a microchannel. This interface may become unstable, it may grow with time, flap one of the walls, and form micro droplets (Ozen *et al.*, 2006). The droplets are reproducible, with very narrow size distribution, and relatively more controllable compared to other methods like T-junctions (Thorsen *et al.*, 2001) or flow focusing device (Gañán-Calvo, 1998). Microfluidic droplets can be generated in the presence of two immiscible phases. The droplet formation mechanism is a non-spontaneous process in the microsystems, various droplet formation methods have been developed in order to control the size, the frequency and the shape of the droplets (Casadevall Solvas and deMello, 2011). These methods are divided into two categories as active and passive. Both methods are based on the deformation due to destabilization of the interface between two immiscible liquids. While passive methods destabilize the interface by manipulating the inertial and viscous forces, active methods do it by applying an external force to induce an instability on the interface. These micro droplets have application areas in chemical reactions (Hatakeyama *et al*., 2006), biology (Song *et al*., 2006) and polymerase chain reaction (de Mello, 2001). Droplet microfluidics has advantageous of high throughput, easy scalability and controllability compared to continuous flow systems (Teh *et al.*, 2008). While the droplet microfluidics continues to extend its application field, the droplet

formation mechanism needs to be improved to have a better control on the size and shape of the droplets.

In this study, various fabrication methods to make microchannels with electrodes, which are placed along the flow direction are investigated and then the channels are designed and fabricated. Then, the instability of the interface between two immiscible and Newtonian liquids which are assumed as incompressible is experimentally investigated. The effect of the electric field subjected normal to the flat interface between the two liquids is studied parametrically in both the linear and the non-linear regime. In the first part, the critical voltage at which the flat interface between the two immiscible liquids starts to be deflected is determined under the effect of a normal electric field. The parameters considered are the flow rate ratio, the depth ratio, the viscosity ratio and the total flow rate. In the second part, the nonlinear evolution of the interface starting from its deflection at its critical voltage until the interface hits the wall of the channel is recorded with a high-speed camera and the behavior of the interface is investigated as a function of the depth ratio, the viscosity ratio, and the total flow rate. Finally, the size of the droplets which are formed after the interface hits the wall of the channel is determined as a function of the depth ratio, the viscosity ratio, and total flow rate.

This thesis begins with a literature survey section on the electrohydrodynamic instability of the interface between two immiscible liquids, and microfabrication methods focusing on microchannels. Then, the experimental procedure is discussed. As the following section, the results for the three parts mentioned above are presented and interpreted. In the last section, the thesis is finalized with the conclusion section and recommendations are presented. An appendix is provided for the derivation for determining the depth ratio as a function of the flow rates, and the computer codes used during the study.

2. LITERATURE SURVEY

In this section, first, microchannel fabrication techniques are discussed in detail. Then, as in our study, the electrohydrodynamic instability and the leaky dielectric model are reviewed. Although the applications of the droplet microfluidics stay out of our research topic, the droplet formation mechanisms are presented since the size of the droplets which are formed due to the electrohydrodynamic instability are investigated in our work.

2.1. Microchannel Fabrication

As in the progress of miniaturizing the integrated circuit systems in the computer industry for the last fifty years, in the field of the chemical and biological analysis a similar progress was achieved. This miniaturizing allowed gathering large scale systems on a single small device (Fiorini and Chiu, 2005). Microfluidic systems have been used for mainly chemical and biological analysis, biodiagnosis, fundamental research, and as tools for biology and chemistry (McDonald *et al.*, 2000).

The applications of the microfluidic devices dictate the use of a certain material and hence an appropriate fabrication method. Apart from the cost and the accessibility, the physical and chemical properties of the material (e.g. wettability, machinability, molecular adsorption, surface charge, elasticity and light transmittance (Becker and Locascio, 2002) are the determinant factor on the decision of the material to be used. The properties of the material are also important for the fabrication processes as well as the application of the devices.

2.1.1. Fabrication Methods

The fabrication process is usually determined according to the material used, since the material's properties may impose certain constraints. For example, while manufacturing with hot embossing, the glass transition temperature at which the material loses its rigid form and transforms into a softer form, has importance on the fabrication process since the material may be deformed while being exposed to a higher temperature than its glass

transition temperature during the fabrication process. The material's properties may also have an effect on the application. For instance, in the application of electroosmotically driven flow, it is required to have an electric field drop across the channel. In order to apply an electric field, electrodes are required but the material of the channel should not conduct electricity. Therefore, the electrical properties of the material become vital for that application (Becker and Locascio, 2002). Below, some very common micro fabrication methods are presented.

The first microfluidic devices were fabricated by using glass or silicone (Terry et al., 1979). These devices were mainly fabricated by micromachining techniques which were firstly used in microelectronic and semiconductor industry. The micromachining techniques such as photolithography, electron beam lithography and etching are mostly performed in laboratories or well-equipped areas which have facilities like clean room and many other equipment (Martynova et al., 1997). Glass was preferred as a material in microfluidic systems, since it has very advantageous physical properties such as light transmittance, compatibility with most of the chemicals and durability. Furthermore, one of the other advantages of the glass is related to the fabrication methods which are well understood and easy to handle (Rodriguez *et al.*, 2003). However, glass is expensive, and the cost of fabrication methods for glass is comparable to other techniques (Fiorini and Chiu, 2005). Therefore, plastics are preferred and used widely in the fabrication process. Another important advantage of the plastics is that they may be modified by adding additives such as fillers, plasticizers, stabilizers and antioxidants, instead of using pure polymers (Becker and Locascio, 2002).

Soft lithography technique, named by Xia and Whitesides (1998) is based on replica molding and a set of steps including the fabrication of a patterned silicon master, soft baking, and exposing to UV light. This technique allows producing polydimethylsiloxane (PDMS) replica molds. The main advantages of this technique are inexpensiveness, rapidness, easiness and reusability of the silicone master (Whitesides *et al.*, 2001).

Thermoset polyester technique is similar to the soft lithography. Instead of PDMS replica molds, thermoset polyester (TPE) which is highly light transmitter, not elastic, and compatible with non-polar solvents is employed. TPE is a direct complimentary of PDMS

since it has properties more advantageous than those of PDMS such as having surface properties stable over periods of hours due to due to exchange of PDMS molecules between the surface and the bulk (Fiorini *et al.*, 2003). In the fabrication process, like in the soft lithography method, also in the thermoset polyester technique, TPE is first semi-cured before a complete cure (Fiorini *et al.*, 2004).

Hot embossing technique is based on heating and applying pressure with a tool similar to a stamp on a layer of thermoplastic, which changes its shape at a temperature close to the glass transition temperature. In this technique, the most common materials used are polymethylmethacrylate (PMMA), polycarbonate (PC), polystyrene (PS) and polyvinylchloride (PVC). Hot embossing is a very easy and a cheap method. However, the prototyping and the resolution is dependent on the replica stamp which is expensive and time consuming to be fabricated (Xu *et al.*, 2000).

Injection molding technique based on injection of a thermoplastic into the cavity of a mold and the cooling of the material below its glass transition temperature. The advantages of this method are its accuracy, its ease of replication and its suitability for mass production (McCormick *et al.*, 1997).

In laser ablation technique, a laser machine removes part of a material, which is a thermoplastic such as cellulose acetate, PMMA, PS and PC. The removing operation is achieved by engraving of the material with heat. Due to the material used in the operation, the intensity of the laser pulse is arranged at a value for the material to reach its melting temperature at the points where the laser touches. This technique has the advantage of having high resolution since it can be controlled by a software on a computer (Roberts and Kumar, 2010).

Paper-based microfluidics is an ensemble of microfluidic systems that use paper as a platform and the principles of the capillary action. There are several techniques (e.g. photolithography (Martinez *et al.*, 2007), wax printing (Lu *et al.*, 2009), knife shaping (Fenton *et al.*, 2009) and inkjet etching (Abe *et al.*, 2008) which are based on the treatment of the paper surface to create a channel for the liquids to flow. The advantages of paper-based microfluidics are low sample volume requirement, ease of use, portability, high

sensitivity and no necessity to a well-equipped laboratory equipment and well-trained manpower. These characteristics have made paper platforms a promising alternative to conventional microfluidic systems (Yetisen *et al*., 2013).

2.1.2. Fabrication of 3D Microfluidic Systems

The techniques mentioned above are mostly for the 2D flow systems, which are usually sufficient for the current industrial applications. On the other hand, the demands are increased and the microsystems are expected to answer more complex problems. 3D microfluidic systems are thought to be one of the solutions for the applications in biodiagnosis and chemical analysis. Chiu *et al.* (2001) designed a 3D microfluidic systems by combining parallel layers on top of each other for maximal clique problems which is a non-deterministic polynomial-time hard problem in computer science. For the fabrication of each layer, photolithography method was used. Jeon *et al.* (2011) also deigned a 3D microfluidic system integrated with valves and a pump by the same method. As a material of patterned layer PDMS was preferred due to its elasticity. In paper-based microfluidic systems, 3D devices were also proposed (Yetisen *et al*., 2013). The fabrication method was based on gathering the layers of patterned papers as in the conventional 3D microfluidic devices.

2.2. Electrohydrodynamic Instability

Electrohydrodynamic (EHD) is the study of the behavior of fluids in the presence of electrical forces. Basically, EHD is the dynamic of the electrically charged fluids (Castellanos, 1998). The effect of electrical charges on the fluid was observed for the first time in the 17^{th} century. In this work (Gilbert, 1600), it was found that the liquids can be attracted by the conductors charged by friction. At those times, Faraday has observed the motion of the insulating liquids under the effect of an electric field (Paillat and Touchard, 2009). Faraday defined these liquid insulators as “dielectrics” in the mid-1800s (Misra, 2011). In 1838, he observed the motion of a dielectric fluid, turpentine, under the effect of an electric field. Later, (Gemant, 1929) hypothesized that liquid motion shows up between two plates due to the space charges (Tobazeon, 1984). Avsec and Luntz (1936) mentioned about the electrohydrodynamic instability between two plates while studying on the effect

of the electrophoretic force on the free charges in the bulk fluid. Since the experimental investigation of the lateral interfacial stability between conducting and non-conducting fluids subjected to a normal electric field by Taylor and McEwan (1965), EHD has been investigated detailly (Turnbull, 1968; Lacroix *et al*., 1975; Fujino *et al*., 1989). Subsequent experimental works (Melcher and Schwarz, 1968; Lin *et al.*, 2002; Ozen *et al.*, 2006; Eribol and Uguz, 2015) and analytical works using the linear theory (Virányi *et al*., 2004; Li *et al.*, 2007; Uguz *et al*., 2008; Bandyopadhyay *et al.*, 2009) investigated the effect of an external electric field on the liquid/liquid interface.

In many chemical and biochemical industries, the liquid systems have more than one phase. Apart from the governing forces such as capillary, inertial, gravitational and viscous forces, the interfacial forces have significant role on the dynamics of the system. Moreover, if the system is under an electric field, the electrical forces are mainly considered as one of the governing forces (Castellanos and Gonzalez, 1998) and they may create an EHD instability on the interface since the electrical charges on the fluid affects the interface. EHD instabilities are very important for many applications such as electrokinetic (EK) assays, electrospray ionization, EHD enhanced heat transfer, EHD pump, electrospray mass spectrometry, electrospray nanoprinting, electro-coalescence and mixing, electrostatic printing and spinning (Chen, 2011). Although, the stability of the interface is desirable for most of the applications, there are certain applications which are based on the instability of the flow. Since the instability of the interface has a critical role for both cases, EHD has taken the attention for the last decades. (Korshidi *et al*., 2010).

The differences between the EK and EHD instability was defined in the works of Melcher and Taylor (1969) and Saville (1997). Hoburg and Melcher (1976) investigated the interfacial instability between two miscible fluids both analytically and numerically under a parallel electric field. They experimentally observed the diffusive fluid conductivity as the bulk-coupled electrohydrodynamic instability model proposes. Furthermore, at high electric fields, a large-scale mixing occurred. Interfacial instability between two miscible liquids with different electrical conductivities has gained more attention after the work of Oddy *et al.* (2001). In that work, the instability was defined as EK instability due to the high conductivity of the liquids and it was found that the interface was unstable when the interface was exposed to either parallel or normal electric field. El Moctar *et al.* (2003) investigated

the EK instability while studying the EK mixing in microscale. Chen *et al.* (2011) and Lin *et al.* (2002) observed a critical electric field above which the interface between two miscible liquids with different electrical conductivities became highly unstable. Chen *et al.* (2003) investigated the importance of the conductivity gradient on the instability of the interface. It was explained by the bulk couple model which is based on a separation in charges in the bulk fluid. Distinctly from the surface coupled model, the charge density in the bulk fluid results in an electrical force which is the driving body force of the instability.

The second approach to analyze the fluid behavior under the effect of an electric field is called the surface coupled model, which is based on the difference in the electrical conductivities of the liquids at the interface. Consequently, there is no gradient of electrical conductivity at the interface as in the bulk couple model, but there is a sharp interface and a jump of all electro-physical properties across that interface. Also, the electrical force is not considered as a body force on the system.

Melcher and Scwartz (1968) observed that the bulk effect might also result in an instability between two liquids subjected to both a tangential and normal electric field. Abdella *et al.* (1996) investigated the electrohydrodynamic instability of two superposed fluids under the normal electric field by making a linear stability analysis. The stability of the planar interface was found as dependent to parameters such as the permittivity ratio, conductivity ratio, viscosity ratio, density ratio, and surface tension.

Thaokar and Kumaran (2005) investigated the interfacial instability of two dielectrics between two plates under a normal electric field. They used linear and weakly nonlinear theory with zero Reynolds number approximation. In this work, it was observed that the interface became unstable when the potential difference on the interface was larger than a critical value. This critical value was observed as being dependent to the ratio of dielectric constants, viscosity ratio, depth ratio of the fluids and the surface tension.

Craster and Matar (2005) investigated the interfacial instability between two leaky dielectric liquids under the effect of a normal electric field. They observed that decreasing the depth ratio has a destabilizing effect on the interface. Uguz *et al.* (2008) made a linear stability analysis of the interface between two leaky dielectric liquids under an electric field

parallel to the flow direction. The stability was analytically investigated for fast electric charge relaxation times.

2.2.1. The Leaky Dielectric Model

In most of the recent studies, while working with immiscible liquids, the interfacial instability between two perfect dielectric liquids or between a dielectric and a conducting liquid (Eow and Ghadiri, 2003) has been investigated. In the systems where two dielectric liquids are used, the interface has no free charge on it. In the systems where a dielectric and a conducting liquid are used, the interface is destabilized due to the presence of an electrostatic energy (Khorshidi *et al.*, 2010). On the other hand, the presence of leaky dielectric liquids complicates the analysis due to quantitative discrepancy between the theory and the experiment (Ha and Yang, 2000), since the possibility of the free charge presence on the interface. Moreover, free charges on the interface may be accumulated and redistributed (Khorshidi *et al.*, 2010). The small rise in the surface charges results in an increase in the instability of the interface. Therefore, the critical voltage becomes less than that expected from the theory based on the systems with perfectly dielectric fluids (Melcher and Taylor, 1969).

The leaky dielectric model, which was developed by Taylor and Melcher (1969) addresses no bulk charge density, but a slight surface charge density on the interface. The fluids are assumed not insulators nor conductors. The weak electrical conductivity creates a tangential stress on the interface while being exposed to an electric field (Saville, 1997).

Shankar and Sharma (2004) studied the effect of an external electric field on the instability of the interface between two thin leaky dielectric films. They used a linear stability analysis and studied the effect of parameters such as the conductivity ratio, the ratio of dielectric constants, the depth ratio and the viscosity ratio. As a result, the viscosity ratio was shown to have a significant effect on the wavenumber of the fastest growing mode in contrast to a system with a perfect and a leaky dielectric liquid couple. Apart from that study, the instability of the interface between two leaky dielectrics also investigated (Craster and Matar, 2005; Thaokar and Kumaran, 2005; Ozen *et al.*, 2006; Uguz *et al.*, 2008). Li *et al.* (2007) found that the ratio of the conductivities and permittivities are the determinant

parameters on the instability of the interface between two leaky dielectric liquids. They observed that in certain cases, the interface could not be destabilized on the contrary of perfect dielectrics. Uguz *et al.* (2008) proposed a diagram based on the electrical conductivity and permittivity ratios of the liquids. The diagram basically indicates whether the interface between the liquid couple can be destabilized or not based on the ratio of conductivities and permittivities of the leaky dielectric liquid couple.

2.2.2. Direction of the Applied Electric Field

The stability of the interface under the effect of an electric field was investigated when the electric field is applied normal (or vertical direction) to the flat interface between the liquids or parallel (tangential) to the flat interface (Eribol and Uguz, 2015). The system under study may be composed of two perfect dielectrics or leaky dielectric liquids. As a result, it was observed that the normal electric field has a destabilizing effect on perfect dielectric model. However, in the leaky dielectric model, the interface may continue to stay stable while being subjected to a normal or parallel electric field. Moreover, in some cases, the parallel electric field could not induce an instability while the normal electric field could.

Uguz *et al.* (2008) provided a phase diagram of conductivity ratio versus permittivity ratio by making a linear stability analysis of two leaky dielelectric liquids subjected to a normal or a parallel electric field. The diagram shows the regions where the interface may be destabilized using a normal or a parallel electric field based on the conductivity and the permittivity ratios of the liquids. Moreover, they found that the destabilizing range of a normal electric field is larger than that of a parallel electric field. In the diagram, there are two regions where neither a normal nor a parallel electric field has a destabilizing effect.

In a subsequent work, Uguz and Aubry (2008), confirmed their previous result and included the magnitude of the growth rate of the instability. Therefore, the regions which indicate that either normal or parallel electric field have a destabilizing effect, are divided into two regions showing which one has a larger growth rate. Apart from these studies, Ersoy (2012) and Nurocak (2013) numerically and Eribol and Uguz (2015) experimentally investigated the direction of the electric field on the interfacial instability.

2.2.3. Direct Current and Alternating Current

Gamphire and Thaokar (2010) studied on the interfacial instability of two immiscible both perfect and leaky dielectric liquids applying alternative current (AC) electric field. A linear stability analysis was performed and the Floquet analysis showed that the frequency has a significant effect on the growth rate of the fastest growing mode and the critical electric field. It was observed that AC field could weaken the present instabilities originating from the system. Furthermore, it was proposed that the growth rate can be arranged in a range between the growth rate in the low frequency limit on a leaky dielectric system and the growth rate in the high frequency limit on a perfect dielectric system. It was also observed that the presence of an AC field leads to instabilities on the stable interface at zero frequency by increasing the frequency of the system.

Roberts and Kumar (2010) investigated the effect of an AC electric field on the size and shape of the pillars which forms after that interface between two thin liquid layers becomes unstable. Since for the perfect dielectric systems, AC behaves like DC electric field, leaky dielectric model was implemented. Linear stability analysis was performed by applying Floquet theory. According to the numerical results, it has observed that the presence of an AC field allows to control the level of accumulation of the free charges on the interface. In a subsequent work, Roberts and Kumar (2010) extended their research to trilayer systems. The EHD instability on the interfaces between polymer/polymer/air liquid trilayer films was studied by performing a linear stability analysis under an AC field. The motivation behind the use of AC was to enhance the control over the pillar formation after the stability was lost. In perfect dielectric systems, the effect of AC showed no difference, however for leaky dielectric model, AC allowed to change instability mode to create complex topography since the controlling the position of free charge within the system was possible.

2.2.4. Droplet Formation

The droplet based microfluidics concentrates on generating droplets and employing them for various applications. Two immiscible phases need to be used since by definition the droplets are bounded by free surfaces and confined in a different environment. One of the phases is called the dispersed phase (droplet) and the other one is the continuous phase.

The mechanism is based on the rupturing of the unstable interface between the continuous and the dispersed phase (Teh *et al.*, 2008).

There are various methods in micro systems to form droplets. Most of these methods which allow controlling the size and the shape of the droplets, can be categorized as passive and active methods (Gu *et al*., 2011). The passive methods such as co-flowing (Nunes *et al.*, 2013), T-shaped junction (Okushima *et al.*, 2004) and flow focusing stream (Anna *et al*., 2003) are based on the flow patterns and geometry of the system which induce the growth of instabilities in the system. The active methods such as thermal actuation (Nguyen *et al.*, 2007), electro-magnetic field application (Tan *et al.*, 2010) and electric field application (Ozen *et al.*, 2006) are based on an external force to induce an instability on the interface.

In active methods such as the electric field application method, the size and the shape of the droplets may be controlled. The controlling mechanism is usually based on controlling a parameter of the driving force on the interface. In an electric field application, it can be the voltage or the distance between the electrodes (Eribol and Uguz, 2015), or the frequency (Gamphire and Thaokar, 2009) for AC electric field applications. However, there are not many studies on the droplet formation based on electric field application. Ozen *et al.* (2006) proposed an electric field application to form monodisperse droplets in two phase liquid system. The interface was subjected to a normal electric field and formed droplets after being destabilized and ruptured. The experiments were performed at various voltage values between 250 and 600V for two different flow rate ratios. It was observed that droplets at different sizes were spaced with certain distance between two droplets. Eribol and Uguz (2015) also investigated the droplet formation in a system of two immiscible liquids. Although the droplet size was not investigated in the work, the instability of the interface which later results in droplet formation was studied. The aim was to find the critical voltage and the electrical number which is a dimensionless number and to see the effect of the parameters which are the flow rate ratio, the total flow rate, the viscosity ratio and the width of the channel on the critical voltage and the electric number.

3. EXPERIMENTAL WORK

3.1. Chemicals

In the experiments, ethylene glycol and various viscosity silicone oils are used. The liquids are chosen such that they are immiscible, non-toxic, compatible with the materials used, and non-evaporative. In addition, the electric field should have a destabilizing effect on the interface. The detailed explanation is discussed in Section 2.2. In order to consider viscosity as a parameter and to make several experiments with different viscosity ratios of the liquid couples, silicone oil of five different viscosities was employed. The list of the chemicals used in the experiments and their electro-physical properties (density, kinematic viscosity, electrical permittivity, and electrical conductivity) along with their brands and the vendors are given in Table 3.1. The listed numbers of all physical properties are assumed at 25^{o}C. The physical properties of ethylene glycol are obtained from MEGlobal (2008). The conductivities of silicone oils are reported by Zhag *et al.* (2006). Relative permittivities of silicone oils are given by Paranjep *et al.* (1935). Rest of the data of silicone oils are given in Shin Etsu Co. (2004). The interfacial tension, γ between silicone oil and ethylene glycol is found as 18 mN/m. (Bico *et al.*, 2000).

3.2. Experimental Setup

All of the experiments were carried out in the same experimental setup which includes a Nikon Eclipse LV100POL optical microscope (Nikon Instruments Europe B.V., Netherlands), a Dual Drive System 33 syringe pump (Harvard Apparatus, USA), a direct current (DC) power supply (Glassman High Voltage Inc., USA), a Fastec InLine high-speed camera (Fastec Imaging, USA), an assembled desktop computer, two 20 mL Fortuna Optima Luer lock tip style glass syringes (Poulten & Graf Ltd., UK), poly ethylene tubing (Scientific Commodities Inc., USA) with an inner diameter of 0.72 mm and an outer diameter of 1.22 mm and green 21G (outer diameter of 0.81 mm) needles and a handmade microchannel. The experimental setup is demonstrated in Figure 3.1a and the schematic presentation is illustrated in Figure 3.1b.

Table 3.1. Electro-physical properties of the chemicals in the experiments.

Chemicals	**Brands / Vendors**	**Density, ρ (kg/m^3)**	**Kinematic Viscosity, ν (cSt)**	**Conductivity, σ (S/m)**	**Relative Permittivity, ε**
Ethylene Glycol	Merck	1100	15	1.1E-04	37.70
Silicone Oil (10 cSt)	Brookfield	930	10	1.0E-13	2.65
Silicone Oil (20 cSt)	Sigma-Aldrich	950	20	1.0E-13	2.70
Silicone Oil (50 cSt)	Brookfield	960	50	1.0E-13	2.72
Silicone Oil (100 cSt)	Brookfield	965	100	1.0E-13	2.74

The microchannels are designed and fabricated in the laboratory and they are made from basically two thick and two thin Plexiglas sheets, both one-sided and double-sided tapes and aluminum tape for the electrode parts of the channel. The detailed manufacturing process is explained in Section 3.3.

The microchannel is placed on the optical microscope. While the light source of the microscope provides enough light to clearly show the interface between the liquid couple, the high-speed camera connected to the microscope records at 250 fps the video by using a computer software (FIMS DEMO 3.0). The computer is used both for saving and watching the videos live. As the objective for the microscope, a 5X and 2X objectives are chosen to have enough FOV (field of view) and to fit the width of the channels into the objective.

The power supply was used to apply voltage between the electrodes of the microchannel. The positive and the ground clamps are clipped to the electrodes. During the experiments while the electrical current control knob stays constant at very close to 0A, the voltage control knob is turned manually to the desired value.

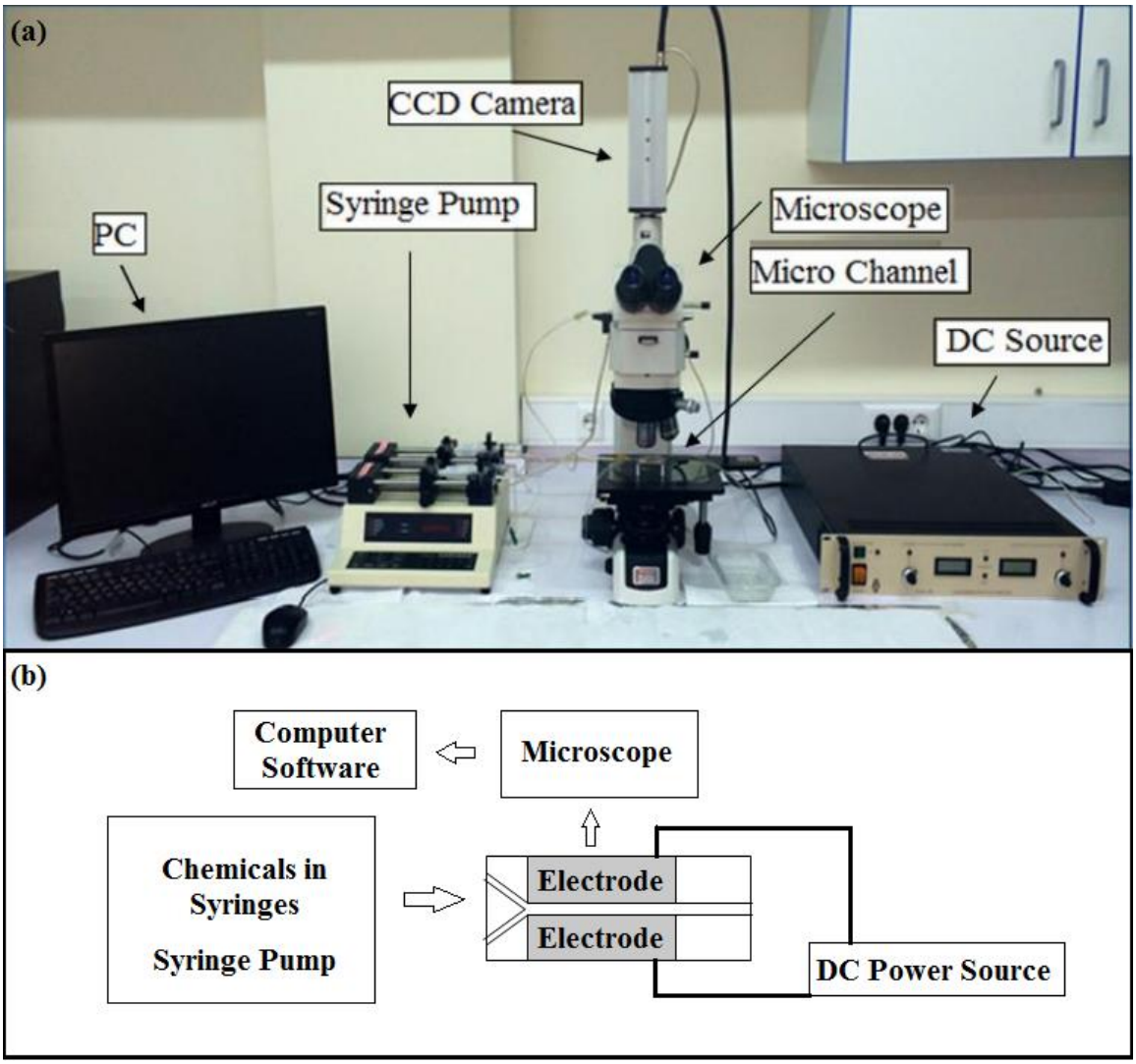

Figure 3.1. (a) Equipment and (b) illustration of the experimental setup.

The syringes with inner diameter of 19.62mm are connected to the microchannel via the tubing and the needles. Syringe pump allows different flow rates for each of the two syringe zones in a range between 13 μL/h -27 mL/min of flow rate.

3.3. Microchannel Design and Fabrication

In order to apply an electric field normal to the flow direction in two-dimensional rectangular coordinate system, the microchannel should have rectangular cross section. The electrodes are planned to be opposing each other at the both sides of the channel walls as in Figure 3.2. Since the experiments require the electric field to be applied normal (perpendicular) to the flat interface between two immiscible liquids, an entering (developing) zone is required for the liquids to be fully developed. Moreover, another zone at the exit of the channel is required for the investigation of the possible droplet formation after the interface was exposed to the electric field. Both of those zones are fabricated by a non-conductive material and the electric field zone is fabricated by a conductive material. For the fabrication process, many designs are proposed and most of them are fabricated until a working and a robust microchannel is fabricated.

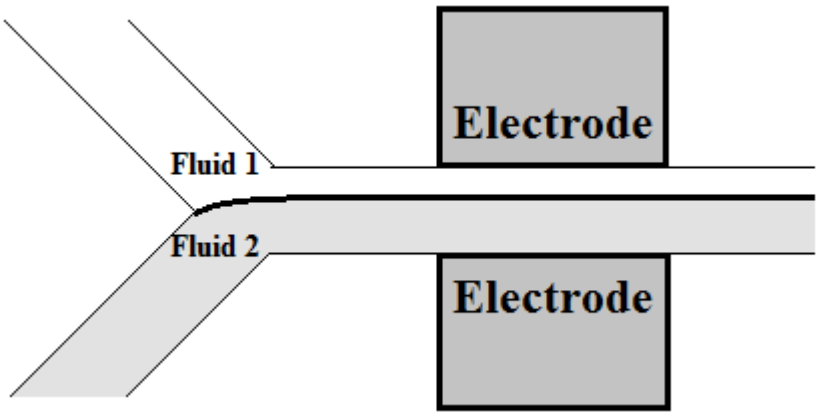

Figure 3.2. Position of the electrodes on the microchannel.

3.3.1. Microchannel with PMMA and Copper Sheets

A 50mm long channel (Figure 3.3) was ordered from a private company (TMR Engineering, Gainesville, FL, USA) and fabricated there. Both of the PMMA sheets were cut and engraved by a computer numerical control (CNC) micro milling machine to form the inlets, the channel, the parts where the electrodes were inserted and the holes where the liquid glue was diffused to fill the space to prevent leakage and to bind the PMMA and the copper sheets (as the conductive material) to each other. The length and the width of the

copper sheets are 30 mm and 15 mm, respectively. The thickness of the channel was chosen as 0.2 mm considering the width (1.1 mm) of the channel. Two stainless steel tubes of 10 mm are inserted into the inlets which a 90^{o} angle in between.

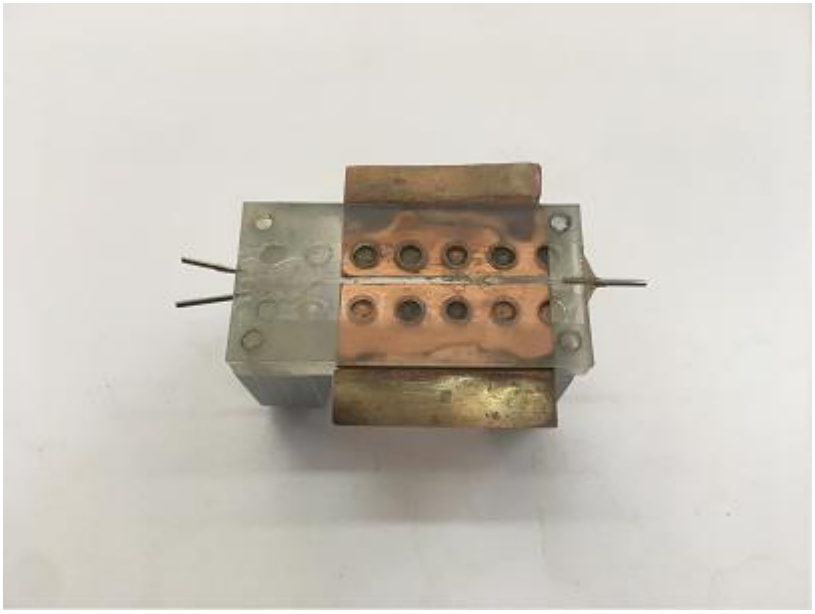

Figure 3.3. Microchannel with PMMA and copper sheets.

This channel was previously used in the group (Eribol and Uguz, 2015) and very satisfactory results were obtained in terms of forming a flat and stable interface, and disturbing the interface with an electric field. However, the channel was blocked with dirt and glue, therefore it was impossible to continue performing the experiments. As the channel was expensive and it took very long time for the shipping, ordering a new channel was not an option. Furthermore, in order to see the behavior of the interface in microchannels with different lengths, it is required fabricating more than one channel in any desired time. Therefore, another channel design is considered.

3.3.2. Microchannel with Gold Coated Glass Slides

The design (Figure 3.4) is based on attaching two gold coated and two non-coated glass slides (Corning Inc., USA) under an ultraviolet light source (Figure 3.5a). In SUNUM laboratory (Sabancı University, Turkey), two of the glass slides with a length of 50 mm, a width of 25 mm, and a thickness of 1 mm were coated with gold by sputtering device. A

standart sputtering device is illustrated in Figure 3.5b. All parts are adhered to each other with metal-metal and metal-glass adhesives (Verifix B 665-0 and 682-T (Bohle Ltd., UK) respectively) activated by ultraviolet light (Figure 3.5c). The lengths of the gold coated parts of the microscope slides, i.e. the electrodes were 30 mm and they were in the middle of the slides. The slides coated with gold were used as the side walls and the non-coated slides as the upper and the lower walls of the channel. In the entrance, a Y-shaped plastic inlet with a 60^{o}C angle was connected to the channel (Figure 3.6a) with the same plastic tubing used in the experimental setup.

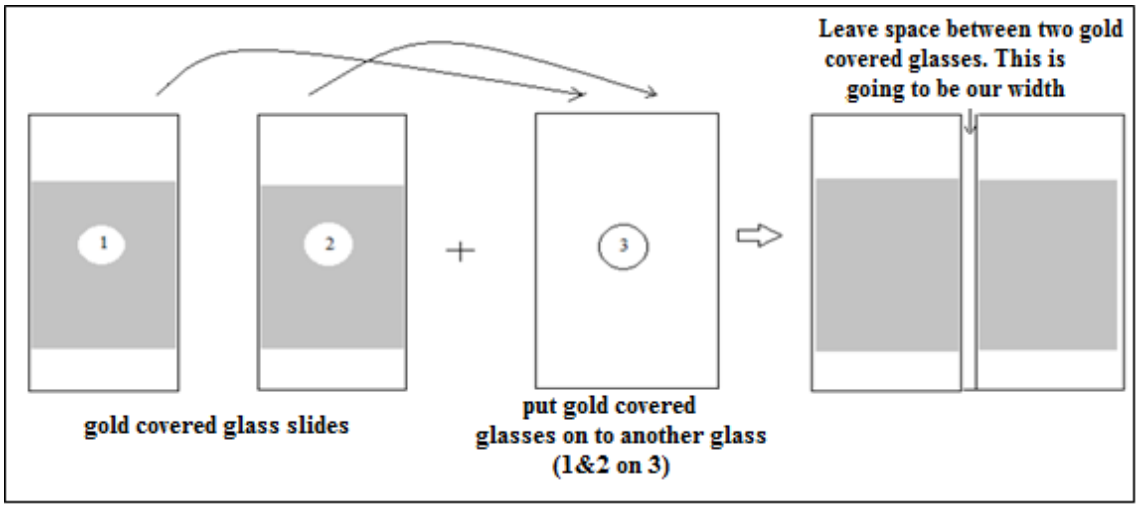

Figure 3.4. The design of the microchannel with glass slides coated with gold.

The width and the depth of the channel were designed and fabricated as 1 mm and the total length of the channel, dictated by the length of the slide was 50 mm. The surfaces of the channel were perfectly flat as the glass slides were used without further processing. However, the problem was the inlet since the interface between the immiscible liquid couple was ruptured when leaving the Y-shaped inlet and entering the glass surfaced channel, which was caused due to the sudden expansion and contraction while passing from the Y-shape inlet. The inner diameter of the Y-shaped inlet was larger than that of the tubing and the inner diameter of the tubing was smaller than the width and the depth of the channel. Therefore, to avoid sudden expansion, several inlets with thin enough walls were designed. An inlet (Figure 3.6b) was designed in SolidWorks (SolidWorks Corp., USA) and planned for fabrication in a 3D printer. However, the current commercial 3D printers are not capable

of printing any layer of material thinner than 1 mm which is almost the same size with the width of the channel.

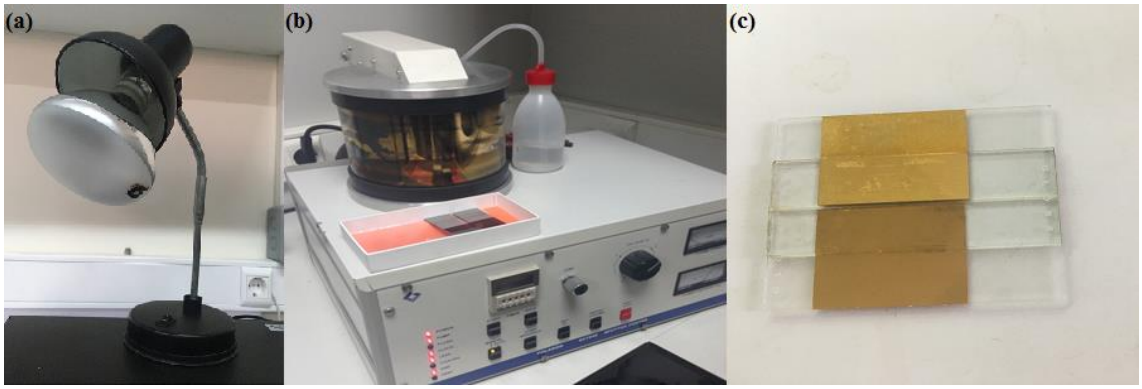

Figure 3.5. (a) The UV light source (b) the sputtering device. (c) The microchannel with glass slides coated with gold.

Another design that was considered included two needles entering side by side into the channel (Figure 3.6c). Even though there might be a sudden expansion for the liquids, there may be a chance to form a flat interface since the two liquids contact each other only after exiting the inlet in the entrance of the channel. That design also failed to form an interface and then a channel with two separate inlets was designed. The plan illustrated in Figure 3.4 was applied to fabricate a channel and the edges of the two coated glass slides which were planned to be the side of the channel was cut with an angle to form a Y-shaped inlet. However, the limitation in that design was the cost of the coating of the glass slides with gold layer and it was observed that the gold layer was etched in time while clipping the positive and the ground clamps to gold coated electrode parts. Thus, an inexpensive channel design was considered to fabricate.

3.3.3. Microchannel with Glass Slides and Metal Sheets

As gold coating required a clean room and sputtering was expensive, metal sheets were considered for the design of the electrodes. The design (Figure 3.7a) was based on piecing seven glass parts whose surfaces were smoothened with a sandpaper and two metal parts together as in Figure 3.7b. First, two 25x50mm glass slides were cut into two, then one of the edges of the two pieces were also cut with a 45o angle. Each glass piece which was cut

was also sandpapered to have a smooth surface. One of the two resting right-angled triangle shaped pieces was used in the inlet part of the channel. All of the pieces were adhered to each other by metal-metal and metal-glass adhesives as described in the previous section. The channel (Figure 3.7c) was leaking as bonding 9 pieces together was not easy. The leaking was due to the gap at the connecting zones of the pieces. Even the small difference in the thicknesses of the metal sheets and the glass slides was the main reason of this gap. In order to avoid the leak, all gaps were filled with low viscosity adhesive (Pattex super glue (Henkel AG & CO., Germany)). Then, the channel worked without any leak. However, thin films were observed on the upper or lower surfaces of the channel. They affected the interface and at certain points of the channel, interface was broken and formed again. It was concluded that glass was not suitable with the chemicals used in our experiments. To change the wettability of the surfaces, various chemicals such as Rain-X glass water repellent (ITW Global Brands Inc., USA) were applied. However, the result was not any better and plastics were considered as the channel material.

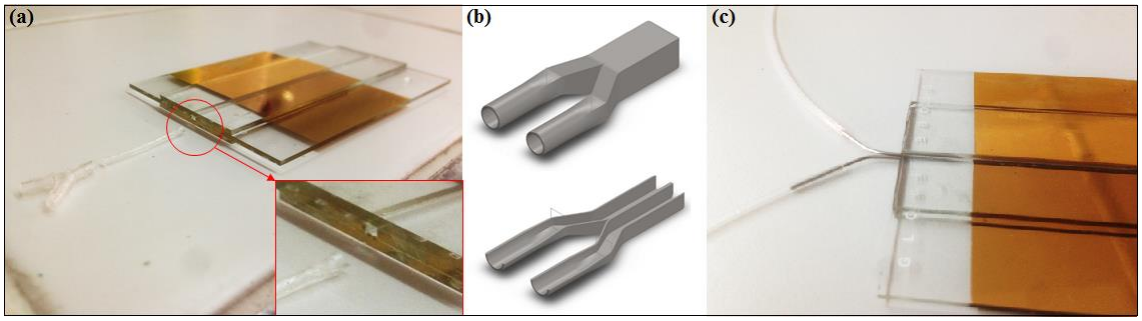

Figure 3.6. (a) The Y-shaped plastic inlet (b) the inlet designed in SolidWorks. (c) The inlet designed with needles.

3.3.4. Microchannel with PMMA and Metal Sheets

After giving up using glass slides, PMMA was preferred since the first channel which was ordered from a commercial company was made of PMMA and worked properly. In order to cut and engrave PMMA, local companies were contacted. There was not any company using micromachining with a CNC machine. 3D Laser cutting and engraving machine (RJ-1390 (Jinan Ruijie Mechanical Equipment Co., Ltd., China)) was used as described in Section 3.3.1. However, the heat released during the process, melted the PMMA

locally as in Figure 3.8a and the walls of the channel became inclined instead of a rectangular channel with parallel and orthogonal walls. Also, on the bottom surface of the channel some ridges are formed due to the laser engraving method (Figure 3.8b).

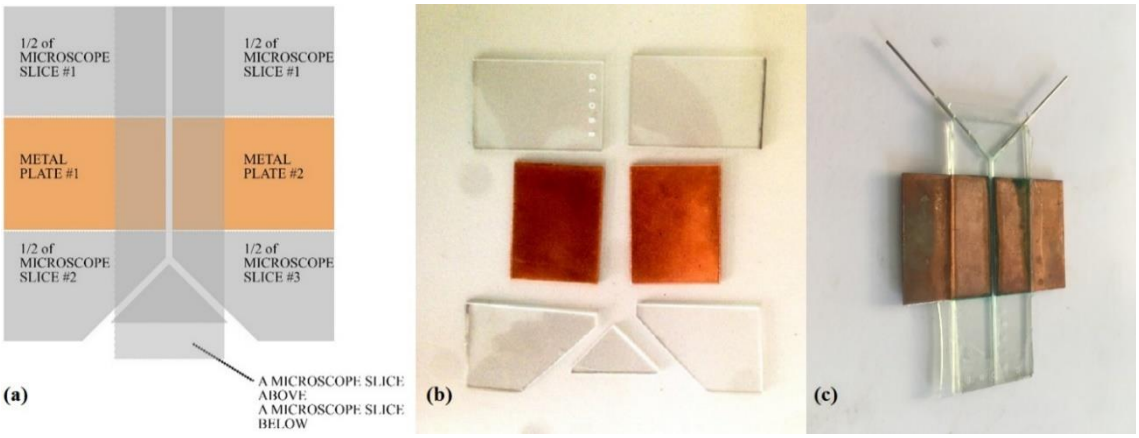

Figure 3.7. (a) The design and (b) the pieces of the microchannel. (c) The microchannel with glass slides and metal sheets

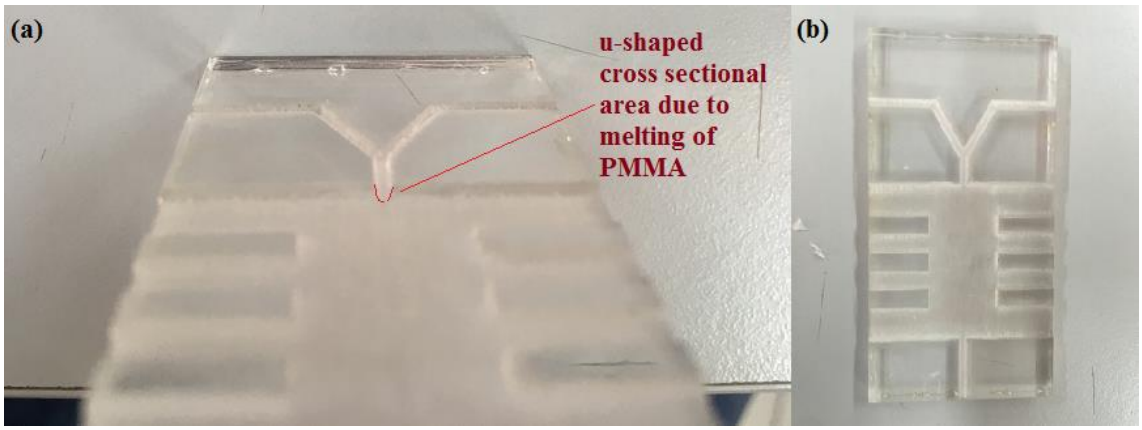

Figure 3.8. (a) Locally melted PMMA. (b) The ridges which formed on the surface of the channel.

3.3.5. Microchannel with PMMA and Tapes

In this design, two PMMA sheets (Koluman Plastik, Turkey) with a thickness of 2 mm, a length of 50 mm and a width of 25 mm, a 0.2 mm thick acetate sheet (Bilgi Dağıtım Kitap, Kırtasiye ve Büro Malzemeleri Tic. Ltd., Turkey) which was cut into two pieces with a

length of 50 mm and a width of 12 mm and three types of tape: (1) double-sided (Tesa Bant Sanayi ve Ticaret A.S., Turkey) with a thickness of 0.03 mm, one-sided (3M, USA) with a thickness of 0.045 mm and aluminum tape (Tesa Bant Sanayi ve Ticaret A.S., Turkey) with a thickness of 0.045 mm were used. The fabrication process of the design (Figure 3.9a) was started by covering the two separate 0.2 mm thick acetate sheets perpendicularly with aluminum tape. The aluminum tapes were covered around the middle part of the acetate sheets. Then the uncovered sides of the acetate sheets were covered again with the one-sided tapes. Therefore, the acetate sheets covered with the aluminum tape on the middle part and covered with the one-sided tapes on the left and right parts had the same thickness everywhere. These two sheets were planned to be the side surfaces of the channel. The middle part covered with aluminum tape was planned to be the electrode for the channel and the other parts covered with one-sided tape were planned to be the entrance and the exit part of the channel. Therefore, the side surfaces of the channel were ready (Figure 3.9b). The two PMMA sheets with a thickness of 2 mm were planned to be the upper and the lower parts. One of the PMMAs was already laser cut to get three holes for two inlets and one outlet. In order to bind these four pieces double-sided tapes were used. Finally, all of the pieces were adhered to each other to have a channel (Figure 3.9c) with a depth of 0.35 mm, a length of 20 mm and a width of 1.1 mm. The length of the electrodes which is decided by cutting aluminum tape in desired width, was chosen as 10 mm. The channel was working without leaking and the desired flat interface was obtained to perform EHD experiments.

3.4. Procedure of the Experiment

(i) Once the experimental setup is ready with clamps attached to the channel electrodes, the desired flow rates are obtained using a syringe pump. The liquids are simultaneously pumped into the microchannel from two separate syringes connected to the microchannel via a PE tubing. The liquids contact each other in the channel and form a flat interface (Figure 3.10a)

(ii) Once a stable interface is obtained, its position is recorded to compare it to its theoretical value (see Section 4.1). Then, the DC power supply is turned on. The control knob of the voltage is turned slowly by hand. The experiment is first done with large voltage increments to roughly determine the critical voltage. Then, at a

second run, the voltage is incremented by 10 V, which is the smallest value shown on the display panel. The interface is recorded using the software FIMS DEMO 3.0 (Fastec Imaging Corporation, USA) and it is followed on the computer screen. An ample time (around 30 seconds for each increment) is given especially close to the critical voltage. The critical voltage values are also recorded with a camera to synchronize with the video of the interface.

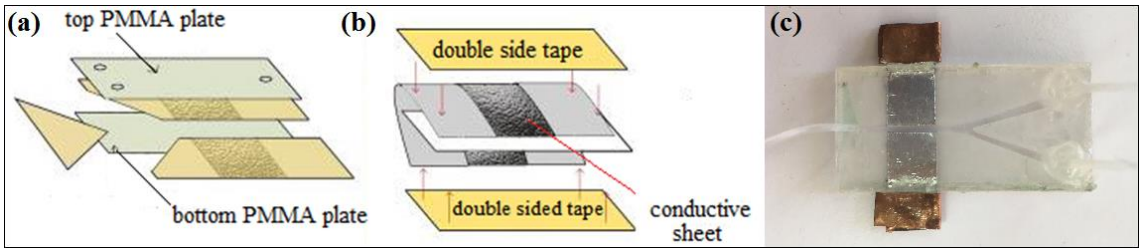

Figure 3.9. (a) The design of the channel with PMMA and tape. (b) The design of the parts which form the side surfaces of the channel. (c) The microchannel with PMMA and tape.

(iii) At the critical value of the voltage, the interface starts to deflect (Figure 3.10b). The deflection is detected through the computer screen by naked eye. However, for some cases it is also tested using image analysis. A 10% deviation from the original position of the interface is taken as the critical voltage. Image analysis and naked eye decision matched perfectly for all cases considered. Once the critical voltage is reached, the deflected interface starts growing. After a very short time (on the order of 100 ms), the interface hits the wall on the side of the silicone oil (Figure 3.10c). Then the interface starts to hit the wall repeatedly (discussed in Section 4.3) and the droplets are formed in the channel (Figure 3.11a and Figure 3.11b). Finally, when the voltage is turned off, the interface starts to regain its flat shape (Figure 3.11c).

(iv) The whole process, starting from the critical voltage to the droplet formation and the restabilization of the interface was recorded.

(v) To verify the results (critical voltage, elapsed time for the interface to hit the wall and the droplet size), the videos (images) are analyzed using MATLAB (MathWorks, USA). Each experiment is repeated at least three times from scratch, i.e. the

experiment is stopped and the channel is cleaned. Also, the experiment is repeated at least three times after the interface is reestablished.

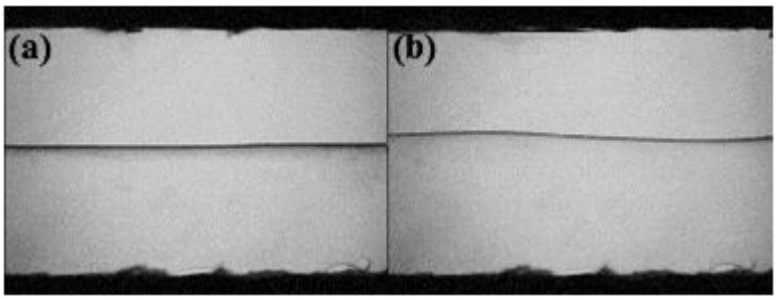

Figure 3.10. (a) The flat interface. (b) The deflecting interface.

(vi) After finishing each experiment, all working equipment is switched off and all plugs are pulled out. The microchannel is cleaned by pumping air into it.

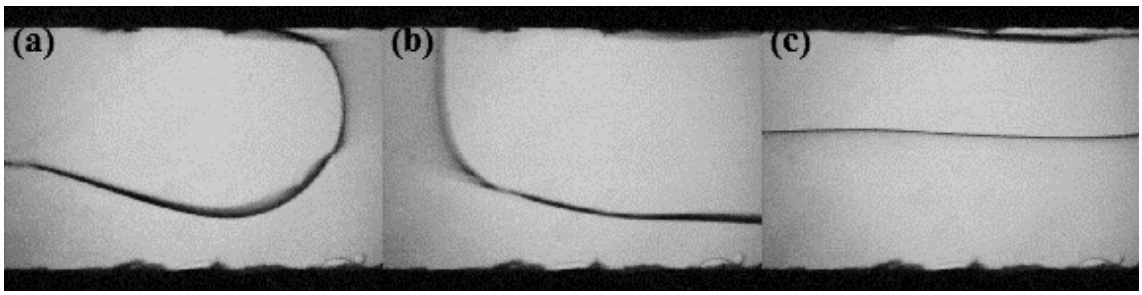

Figure 3.11. (a) The droplet formed in the channel. (b) It moves with flow. (c) The interface regains its flat shape after the voltage is turned off.

3.5. Data Analysis

The recording was done with 250 fps and then the videos were converted to images (one image for single frame) by using a computer software called VLC Player (VideoLAN, France). Then, the interface was located as pixels by using a computer code given in the appendix section. The code was written in MATLAB and was based on scanning the intensity of each pixel. The working principal of the code is based on the scanning the pixels from top to bottom. Since the scanning of the first column which represents the first line of pixels from top to bottom. Once the darker points (higher intensity) which signify the

location of the interface are detected on the first column, the positional average of these pixels are recorded. Then the pixel found on that average position is recorded. Then the code automatically passes to next pixel on the next column. To detect the location of the interface on the second column, the code scans the five pixels below and above that pixel on the second column. After the position of the interface is detected on the second column, the scanning continued for the next columns. All darker points are recorded and the code is able to draw the position of the interface in the width direction of the channel as a function of position in the flow direction. The visual representation is shown in Figure 3.12. This code was executed for all of the images taken from the videos.

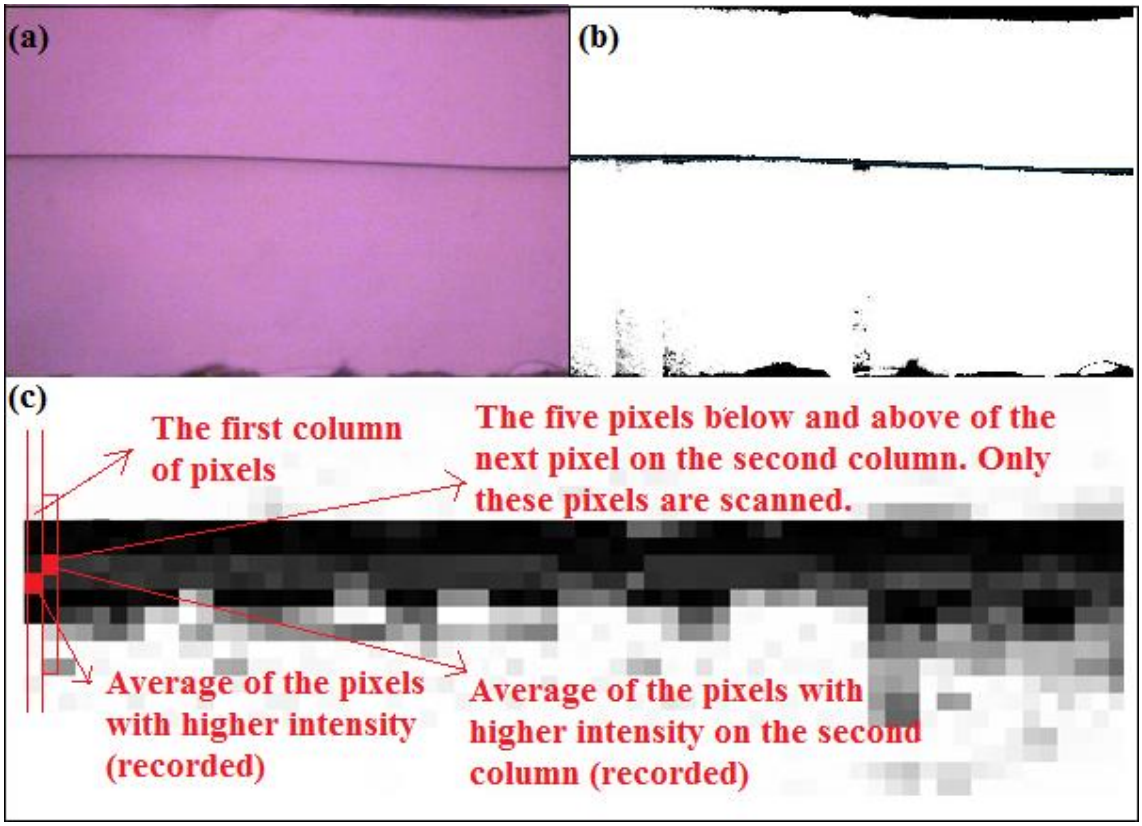

Figure 3.12. (a) The recorded image of the interface. (b) The illustrated intensity profile of the interface. (c) The visual representation of the working principal of the code.

The frame where the interface is started to deflect, is decided by using the code. That frame is decided according to the change in the position of maximum point of the interface. One the interface is moved as that the thickness of one liquid (silicone oir or ethylene glycol)

changes at least 10%, the voltage value applied at that time is decided as the critical voltage value.

Secondly, for the nonlinear analysis part, the time passing from the first deflection till the interface hitting to the wall is decided by the same method. The position of the maximum point on of the interface is recorded with the corresponding time after the first deflection occurs. In order to standardize the data for each experiment, the data which corresponds to the elapsed time during the less thanup to 10 percent change in the position of the maximum point on of the interface is got rid of and don't placenot presented in the results. The time elapsed after 10% change during the bigger changes areis recorded. Therefore, the time dependent positional change of that point is obtained.

For the data which shows the effect of voltage on the droplet formation, the images of the droplet flowing in the channel, are obtained from the frames of the videos. The size of the droplets is first calculated as area on two dimensional images by using ImageJ. Then the areas are multiplied by the depth of the channel. The curvatures in the direction of the depth are not taken into consideration.

The models for the linear theory analysis and the droplet formation are obtained by linear curve fitting on Excel (Microsoft Software, USA).

4. RESULTS AND DISCUSSION

In this section, the effect of the parameters mentioned below on the critical voltage (CV), on the time dependent evolution of the interface from its first deflection until its first hit to the wall and on the size of the droplets are investigated and discussed. The parameters are

(i) Viscosity ratio, μ_r which is the ratio of the first liquid's viscosity $\mu^{(1)}$ to the second liquid's viscosity $\mu^{(2)}$.

(ii) Flow rate ratio, Q_r which is the ratio of the first liquid's flow rate $Q^{(1)}$ to the second liquid's flow rate $Q^{(2)}$. This parameter, as explained in the results, is interchangeably used with the depth ratio H_r of the liquids.

(iii) Total flow rate, Q which is the sum of $Q^{(1)}$ and $Q^{(2)}$.

Note that liquid (1) is taken as silicone oil of various viscosities and (2) is ethylene glycol.

For the critical voltage and the droplet size, empirical models are also established. For these models instead of using the flow rate ratio Qr, the depth ratio Hr, which is the ratio of the first liquid's width $H^{(1)}$ to the second liquid's width $H^{(2)}$ in the channel is used. The reason of that is discussed in detail in Section 4.2.4.

When the interface between two immiscible liquids is exposed to an electric field, it may start to deflect and may be ruptured as a conclusion of the deflection. This rupture may also give rise to micro droplet formation. In order to investigate the behavior of the interface subjected to a normal electric field, first a flat interface is formed between the immiscible liquid couple and the voltage is applied by using a direct current (DC) power supply to create an electric field normal to the interface. In our experiments, silicone oil and ethylene glycol liquid pair is used. A parametric analysis on the critical voltage (CV) is investigated.

In Figure 4.1, the time-dependent behavior of the interface under the normal electric field is shown. In that experiment, 50 cSt silicone oil is at the top and ethylene glycol at the bottom. It should be noted that this is a top view; hence, in the experiment the liquids flow side by side as the effect of gravity is negligible at micro scale. The viscosity ratio in this experiment is 2.929. The flow rates are 50 and 250 μL/min for silicone oil and ethylene glycol, respectively. These flow rates correspond to a flow rate ratio of 0.2 and a depth ratio of 0.45. In Figure 4.1a, where the flat interface is already established, the voltage is started to increase from 0V very slowly (as described in Section 4.3) until the first deflection of the interface appears as in Figure 4.1b. At that point, the voltage is at 300V, which is named as the critical voltage (CV). The voltage is fixed at this critical value for the rest of the observation. For Figures 4.1c, 4.1d and 4.1e, the deflection of the interface grows towards the ethylene glycol side until the interface reaches its minimum point as in Figure 4.1f. After that point, the maximum point of the interface starts to move very fast (0.24 s) towards the silicone oil side as in Figure 4.1g. In Figure 4.1h, the interface is ruptured and it hits the wall. Since the speed of the hitting is very fast (on the order of 0.01 s), the interface is very blurry as the camera cannot catch the image even at 250 fps. Immediately after the hit (Figure 4.1i), ethylene glycol encapsulates the silicone oil as in Figure 4.1j; therefore, silicone oil droplets are formed in the ethylene glycol flow as in Figures 4.1k, 4.1l, 4.1m, 4.1n and 4.1o. In Figure 4.1p, the power supply is turned off and the voltage is at 0V. Since that moment, the interface starts to regain its flat shape and move to its original position (Figures 4.1q, 4.1r and 4.1s). Then, the interface starts to oscillate as in the first deflection before the rupture. Finally, in Figure 4.1t, the interface regains its flat shape and comes to its original position.

For that experiment, the critical voltage is determined as 300V by naked eye. However, the critical voltage observed by naked eye and obtained via MATLAB matched for the cases (tests) done. As the critical voltage is determined with small increments in voltage and ample time is given at each increment, it is not very difficult to determine the first deflection by naked eye. However, for many cases the critical point is also checked with MATLAB.

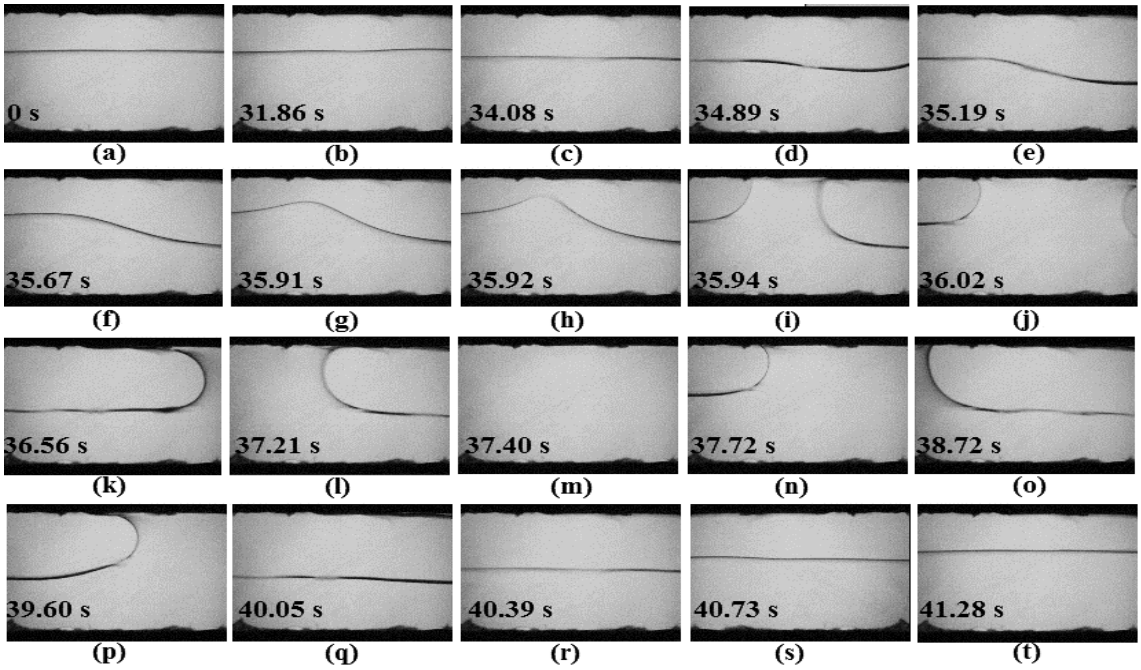

Figure 4.1. The instability at the interface between silicone oil (top) and ethylene glycol (bottom). The critical voltage is 300V. $Q^{(1)}$: 50μL/min, $Q^{(2)}$: 250μL/min and μr: 2.929.

4.1. Investigation of the Depth Ratio

Before performing the stability experiments and investigating the nonlinear evolution of the interface and the droplet formation, the correctness of the depth ratio of the interface which corresponds to a flow rate ratio and a viscosity ratio is determined. To do that, experimentally measured depth ratios are compared to those obtained from the theory pertaining to pressure-driven flow in microchannels. The depth ratio depends on the flow rate ratio and the viscosity ratio of the liquids (see Appendix). The theoretical depth ratio of the interface for any flow rate and viscosity ratios is calculated by executing a computer code on MATLAB.

For several flow rate ratios between 0.11 and 4 at different viscosity ratios, the experimental and theoretical depth ratios were compared at four different viscosity ratios. In Figure 4.2, the experimental depth ratio results are shown for silicone oil and ethylene glycol liquid couple at viscosity ratio of 0.556, 1.183, 2.929 and 5.885.

In Figure 4.2, the experimental depth ratios along with standart error bars and the theoretical depth ratios are given. The experiment and the theory match perfectly except at high flow rate ratio. Therefore, it can be said that in the absence of an electric field, the set up works as expected.

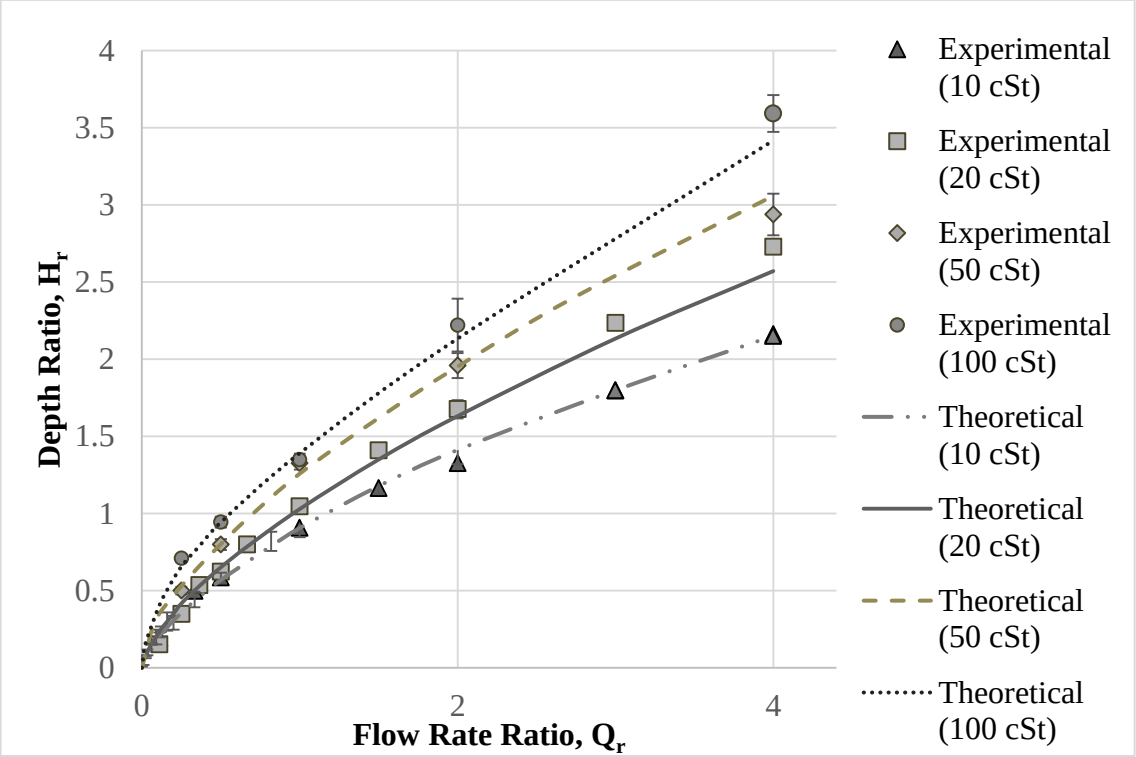

Figure 4.2. Comparison of the theoretical and experimental depth ratios, Hr for the silicone oil/ethylene glycol at μr of 0.556, 1.183, 2.929 and 5.885.

4.2. Determining the Critical Voltage

In the next section, the critical voltage (CV) is investigated for parameters such as the viscosity ratio μr, the flow rate ratio Q_r, and the total flow rate Q.

4.2.1. The Effect of the Viscosity Ratio

In this section, the effect of the viscosity ratio μ_r, i.e. the ratio of the viscosity of silicone oil to the viscosity of ethylene glycol, on the critical voltage is examined for various

volumetric flow rate ratio Q_r. In all these experiments, the total flow rate Q is fixed to 300 µL/min.

In these experiments, ethylene glycol and 4 different silicone oils were used. The only difference of the silicone oils are their viscosities. Other physical properties of the silicone oils are very similar to each other (see Table 3.1). The corresponding viscosity ratios μ_r are 0.556, 1.183, 2.929 and 5.886 and 5 different flow rate ratios Q_r, i.e. 0.25, 0.5, 1, 2 and 4 were used.

The effect of the μ_r on the critical voltage is shown in Figure 4.3. The results indicate that an increase in μ_r results in an increase in the critical voltage, which can be attributed to the stabilizing effect of μ_r. This correlation between the viscosity ratio and the critical voltage is observed for 5 different Q_r. Another result obtained from Figure 4.3 is that the increase of the critical voltage gradually decreases with an increasing μ_r.

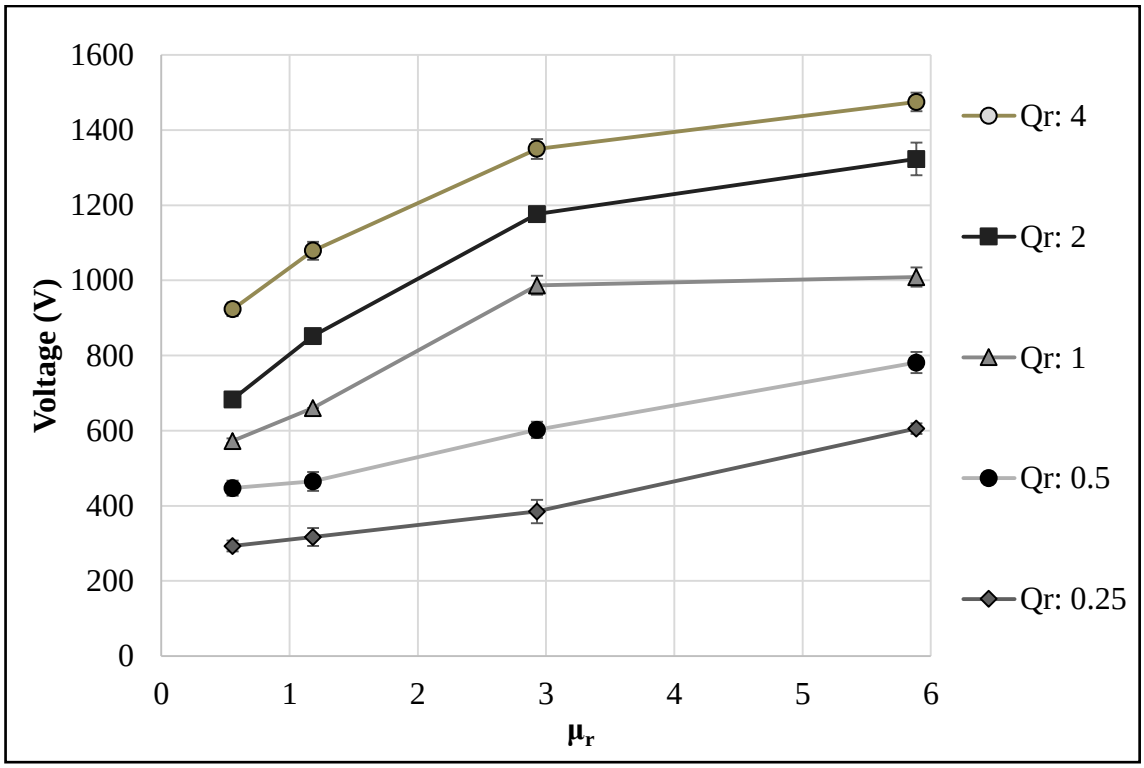

Figure 4.3. The effect of µr on the critical voltage at different Qr.

The critical voltage can also be shown in terms of a dimensionless voltage, named as dimensionless electric number E_b by Uguz *et al*. (2008). The definition of the E_b is given as

$$E_b = \frac{\varepsilon_0 V^2}{\mu^{(2)} H^{(2)} U} \tag{4.1}$$

where ε_0, V, $\mu^{(2)}$, $H^{(2)}$ and U are the vacuum permittivity, applied voltage, the viscosity of the second liquid (ethylene glycol), the height of the second liquid and the characteristic velocity which is defined as $\gamma/\mu^{(2)}$ respectively. Here γ is the interfacial tension between the liquid couple, it is 18 mN/m. Figure 4.4 shows the effect of μ_r on the critical E_b (C E_b) for various Q_r. As can be deduced from Equation 4.1, there are two important differences between plotting the critical voltage and E_b. First, the voltage is squared in E_b. Second, E_b contains the height of the ethylene glycol, i.e. $H^{(2)}$, which is not constant as the μ_r changes. Consequently, even though as μ_r increases E_b increases but the increase might not be same or similar to the increase in the critical voltage.

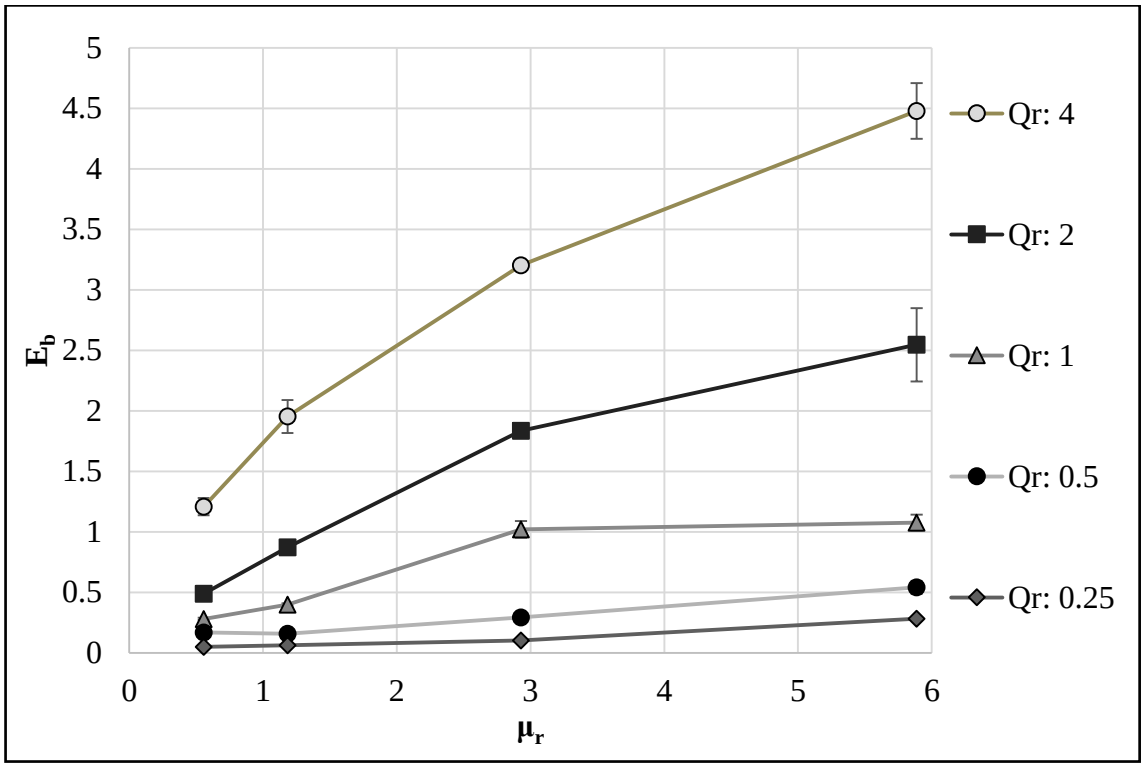

Figure 4.4. The effect of μ_r on the critical E_b at different Q_r.

4.2.2. The Effect of the Flow Rate Ratio

In this section, the effect of the volumetric flow rate ratio Q_r, i.e. $Q^{(1)}$ (SO) /$Q^{(2)}$ (EG) on the critical voltage is investigated at four different μ_r of silicone oil/ethylene glycol liquid couple. In all these experiments, the total flow rate, Q is fixed to 300 μL/min. The values of the parameters are kept same as in Section 4.2.1, i.e. Q_r of 0.25, 0.5, 1, 2 and 4 and μ_r of 0.556, 1.183, 2.929 and 5.886.

The effect of the Q_r on the critical voltage is shown in Figure 4.5. This figure is very similar to Figure 4.3. However, it is easier to observe the effect of the flow rate in Figure 4.5. The results indicate that an increase in Q_r results in an increase in the critical voltage. This increase is due to the stabilizing effect of the silicone oil. As Q_r increases silicone oil occupies more of the channel and the interface becomes more stable, similar to the argument used for the viscosity ratio in Figure 4.4. This correlation between the Q_r and the critical voltage is observed for 4 different μ_r. However, even though one of the μ_r is smaller than 1, the behavior doesn't change.

The effect of μ_r on the critical electric number, C E_b is shown in Figure 4.6. The relation between the μ_r and the critical E_b differs from that between μ_r and the critical voltage. Despite the fact that the critical E_b and the critical voltage has positive relation with Q_r, the critical E_b has a relation close to a linear one with Q_r while the increase of the critical voltage gradually decreases with an increasing Q_r. The difference is obvious when μ_r is 5.886 and 2.929 for V and E_b are compared. The curves for E_b at μ_r of 0.556 and μ_r of 1.183 cross each other. The reason behind that can be based on the thickness of the ethylene glycol, $H^{(2)}$ which is little less than the expected theoretical value.

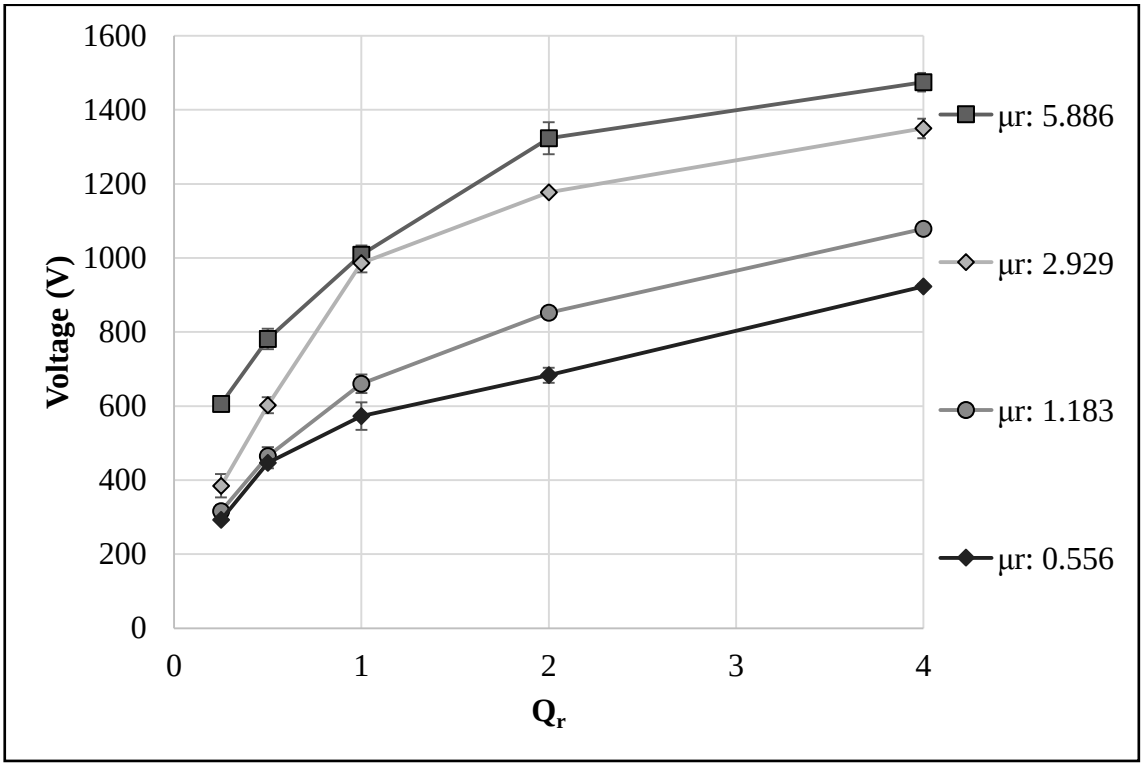

Figure 4.5. The effect of Q_r on the critical voltage at different μ_r.

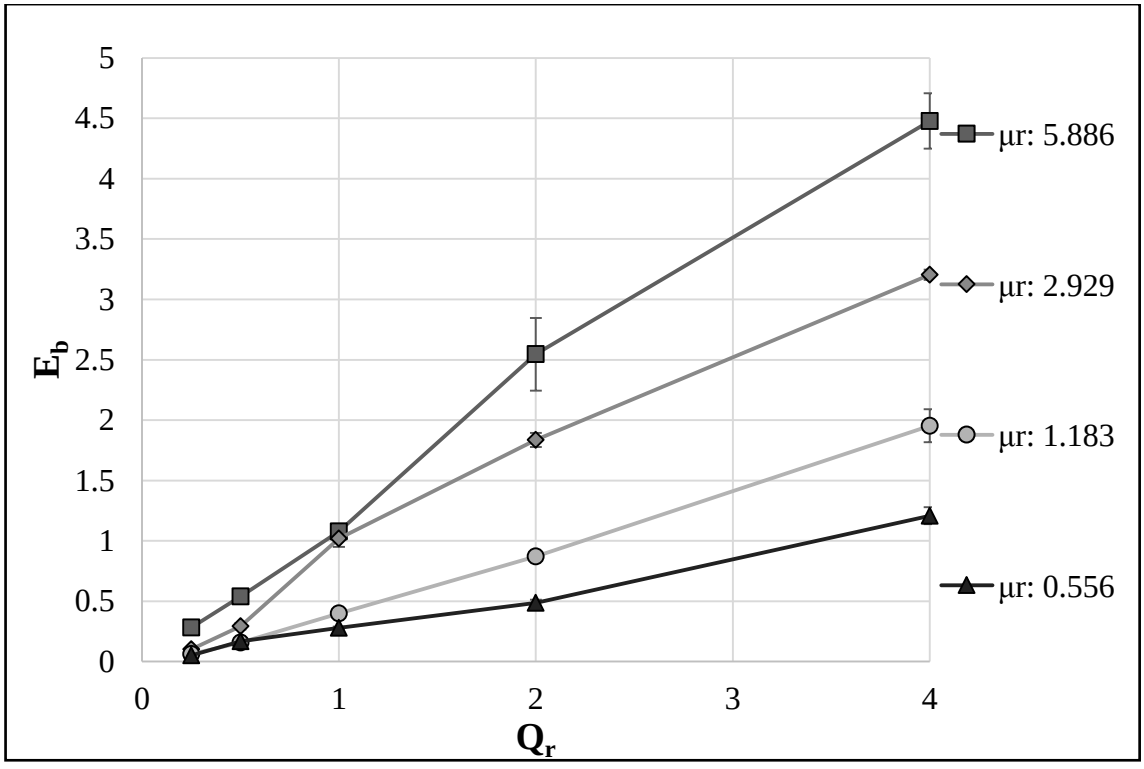

Figure 4.6. The effect of Q_r on the critical E_b at different μ_r.

4.2.3. The Effect of the Total Flow Rate

In this section, the effect of the total flow rate Q on the critical voltage to destabilize the interface between 50 cSt silicone oil and ethylene glycol is examined for various volumetric flow rate ratios Q_r. Note that the viscosity ratio is fixed at 2.929 in all these experiments.

The total flow rate Q in these experiments is chosen as 100, 200, 300 and 400 μL/min. These parameters are used at five different Q_r which are 0.25, 0.5, 1, 2 and 4.

The effect of the Q on the critical voltage is shown in Figure 4.7. The results indicate that the Q has no effect on the critical voltage as also shown in Eribol and Uguz (2014). Hence, the critical voltage is determined by the flow rate ratio and not by the individual flow rates. This correlation between the Q and the critical voltage is observed for 5 different Q_r.

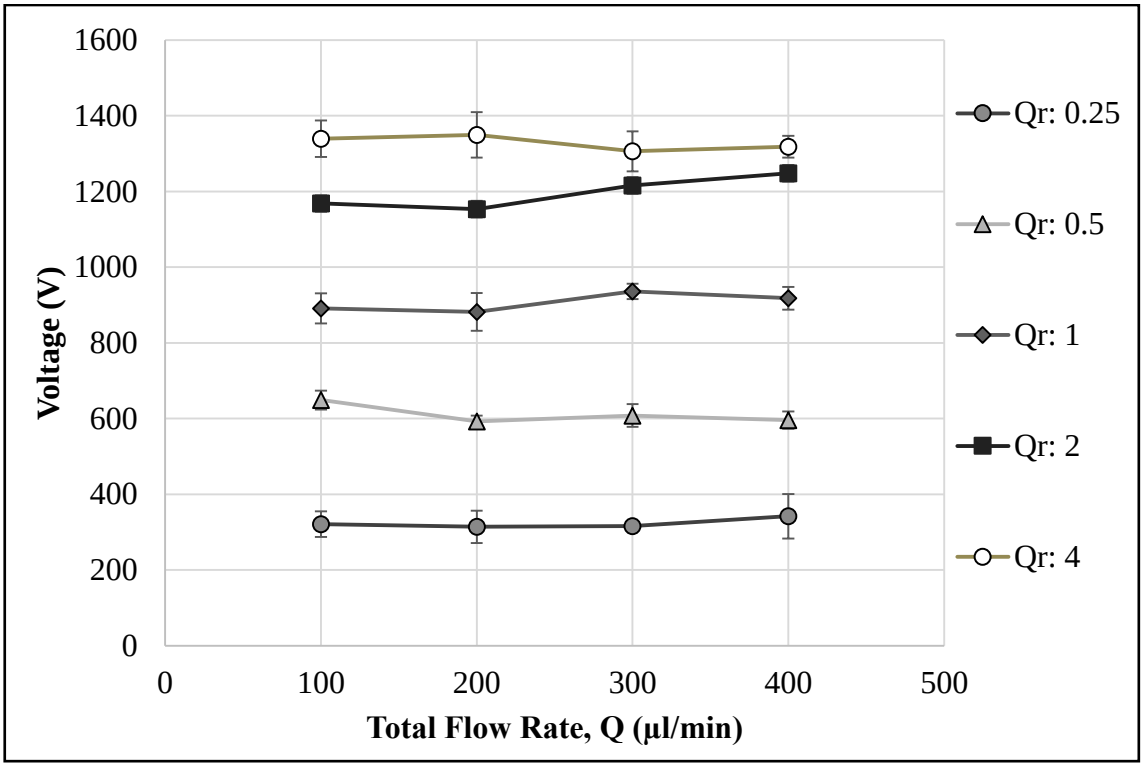

Figure 4.7. The effect of Q on the critical voltage at different Qr.

The effect of the Q on the critical electric number, E_b is shown in Figure 4.8. The relation between the Q and the critical E_b is same with that between Q and the critical voltage because this time as the total flow rate changes the depths of the liquids remain constant.

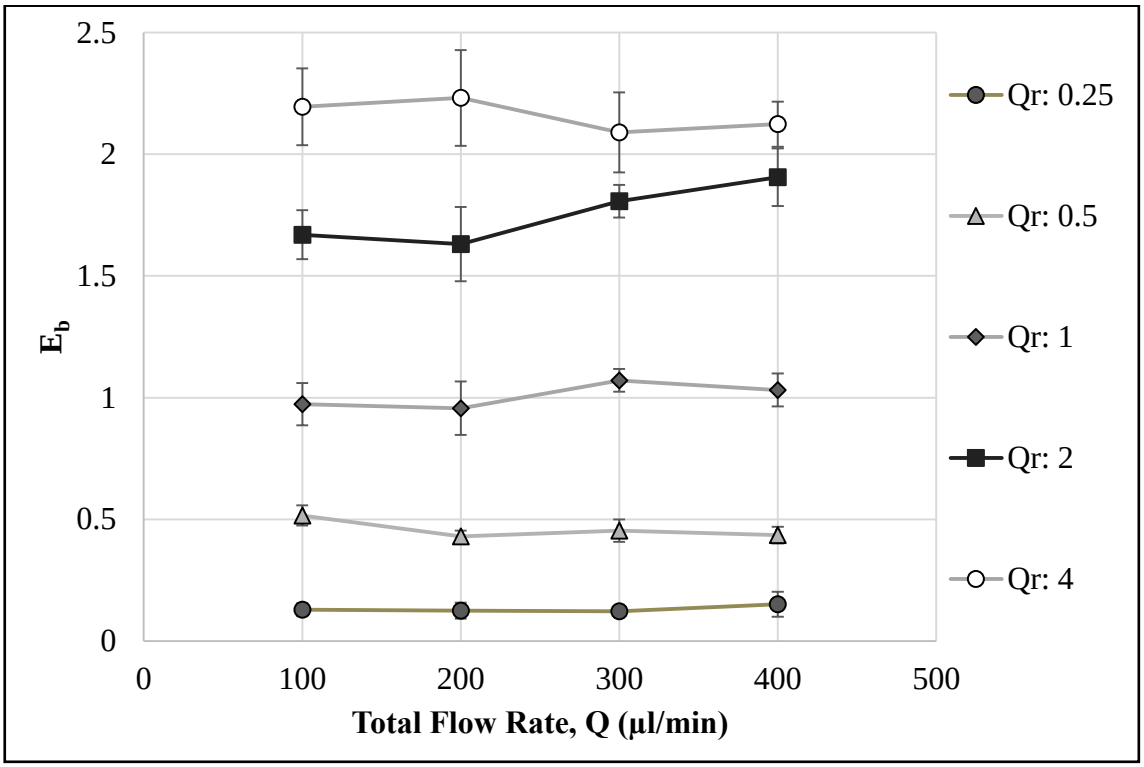

Figure 4.8. The effect of Q on the critical E_b at different Qr.

The error bars for the Q_r: 0.25 are higher than those of other flow rate ratios, Q_r. The reason is that the range of the critical voltage data which are obtained experimentally increases for the higher Q_r and the voltage is squared in E_b.

4.2.4. Empirical Model for Critical E_b

In this section, the aim is to express the dimensionless critical voltage, i.e. the electric number E_b in terms of all parameters studied, i.e. the viscosity ratio μ_r, the flow rate ratio Q_r, and the total flow rate Q. First, in Fig 4.7 it is seen that the total flow rate does not affect the critical voltage. Second, even though Q_r is an input in all experiments, numerically the depth ratio H_r is preferred (Uguz and Aubry, 2008). Once the viscosity ratio is known one can

easily deuce H_r from Q_r (see Appendix). Hence, the empirical relationship is expressed in terms of the depth ratio H_r. In all experiments H_r was also measured.

The experiments are carried out for μr of 0.556, 1.183, 2.929 and 5.886 and Q_r in a range between 0.11 and 0.9 (hence for several Hr, measured in the experiments). Figure 4.9 shows a linear fit of the model. The factors and the coefficients of the model were determined using polyfit function in MATLAB.

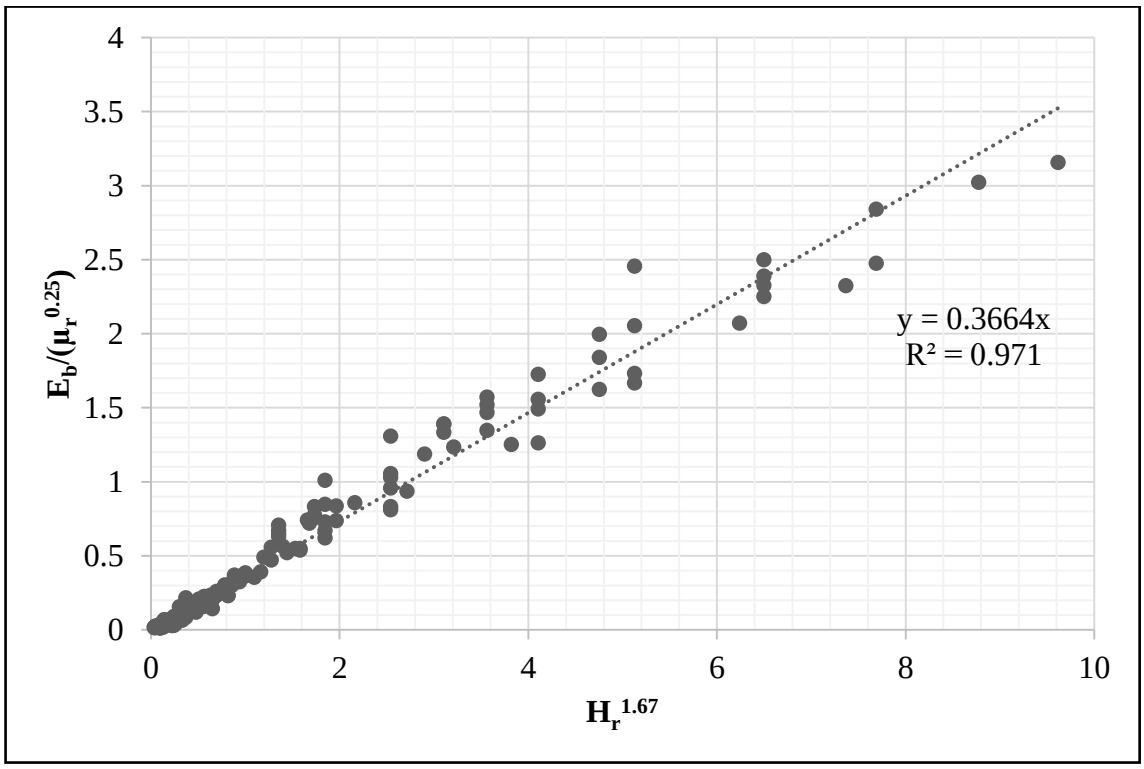

Figure 4.9. The linear fitting for the empirical model of critical E_b as a function of H_r and μ_r.

As seen in Figure 4.9, the critical E_b is a function of μ_r with a power of 0.25 and H_r with a power of 1.67. Therefore, the empirical model can be expressed as below.

$$\text{Critical } E_b = 0.3664\, {H_r}^{1.67} {\mu_r}^{0.25} \tag{4.2}$$

As discussed in Section 4.2.2, the empirical equation shows that the effect of H_r is more dominant than the μ_r on the determination of the critical E_b.

4.3. Evolution of the Interface Deflection

The experiment in Figure 4.10 shows the mechanism of the evolution of the interface deflection. In the figure, the black parts are the electrodes and the channel which stays between the black parts is under the effect of an electric field. The flow direction is from left to right. In this experiment, the flow rates of 50 cSt silicone oil (top) and ethylene glycol (bottom) are 100 and 200 μL/min, respectively. The flow is as laminar since the Reynolds number is between 0.19 and 1.25. The experiment is carried out at a critical voltage of 610V. At the critical voltage value, the flat interface starts (Figure 4.10a) to deflect and to oscillate (Figure 4.10b). The amplitude of the oscillating interface grows by time until the interface tapers at a point. Then, this sharp point almost like a kink, hits the wall extremely fast and the interface ruptures at that point. In our experiments, the first point where the interface, which is like a kink hits the wall is just outside of the outlet of the electrode (Figure 4.10c). For the next hits (Figures 4.10d and 4.10e), the point where the interface hits the wall moves toward the inside of the electrodes. It continues to move until the beginning of the electrodes. Then (after around 5-10 hits, i.e. droplets), the interface continues to hit periodically the wall at the same point. In this way, uniform droplets are formed.

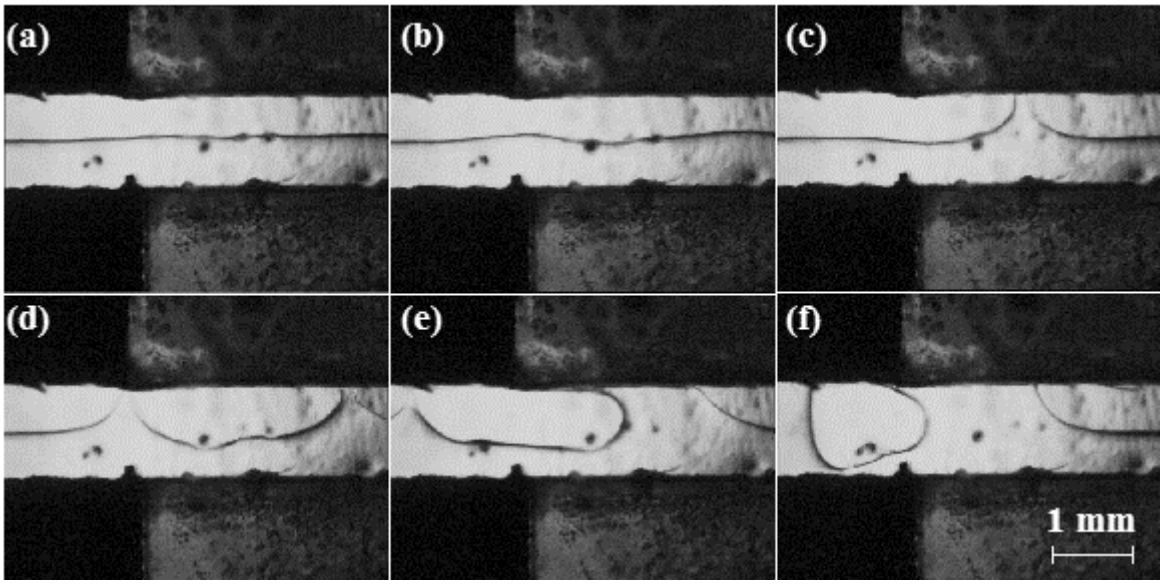

Figure 4.10. (a) The flat interface. (b) Interface deflects. (c) The interface hits the wall for the first time. (d) While the ruptured part moves with the effect of the flow, interface hits the wall for the second time. (e) The third hit occurs. (f) The droplets are formed.

In this part of the study, it is aimed to measure the time elapsed between each periodical hit of the interface and the temporal change in the amplitude of the interface. The results are obtained for different total flow rates. The effect of the total flow rate on the time evolution of the interface between the critical point, i.e. when the interface starts deflecting and the rupture of the interface is investigated. In these experiments, 50 cSt silicone oil and ethylene glycol are used at a volumetric flow rate ratio Q_r of 0.5 which corresponds to a Hr which is around 0.789. The viscosity ratio μr is 2.929. The total volumetric flow rate Q is set to 225, 300, 375 and 450 μL/min.

The effect of Q on the elapsed is shown in Figure 4.11. The results indicate that an increase in Q shortens the time elapsed for the first hit. As seen in the figure, the hitting after oscillations occurs extremely fast, around 0.1s. The sinusoidal behavior of the curve is based on the oscillating movement of the interface. The amplitude of the interface, defined as the difference between the maximum and the minimum position of the interface is around 100 μm even when the interface is assumed flat and stable. The reasons may be that the channel and the frame of the camera are not perfectly parallel to each other and the surface of the channel which is not perfectly flat creates local elevations on the interface. Another observation from Figure 4.11 is that the frequency of the oscillating movements just before the final bounce is larger when the total flow rate, Q is larger. On the other hand, the shape of the oscillations (waves) is similar to each other.

4.4. Droplet Formation

When the interface between two immiscible liquids starts to deflect and ruptures under an electric field, one of the liquids is trapped in the other one as a droplet. As the liquids are subject to a pressure gradient in the channel, the ruptured interface also moves in the channel. Then, the interface is ruptured again from another point in the channel; two ruptured points coalesce and form a droplet. The formation mechanism of the first few droplets was explained in Section 4.3. As mentioned, after the first hit the point where the interface hits the wall moves toward the inside of the electrodes until it is close to the beginning of the electrodes. From that moment, the interface starts to hit periodically the same point in the channel. Therefore, the droplets become monodisperse and ready to be observed. The mechanism of the monodisperse droplet formation including the periodical hits of the

interface is shown in Figure 4.12. For this experiment, 50 cSt silicone oil and ethylene glycol are used. The interface (Figure 4.12a) which is already ruptured at a point closer to the end of the channel (last hit before the periodical hits), ruptures hitting the wall under the effect of the electric field (Figure 4.12b). The ruptured point on the interface starts to diverge and two separated branches of the interface move away from each other while still moving along the channel with the effect of flow (Figure 4.12c). The interface ruptures again at the position where the periodic hits occur as seen in Figure 4.12d. The next ruptured point also starts to diverge in Figure 4.12e and the two close diverged branches of the interface coalesce to form a droplet while moving along the channel as in Figure 4.12f.

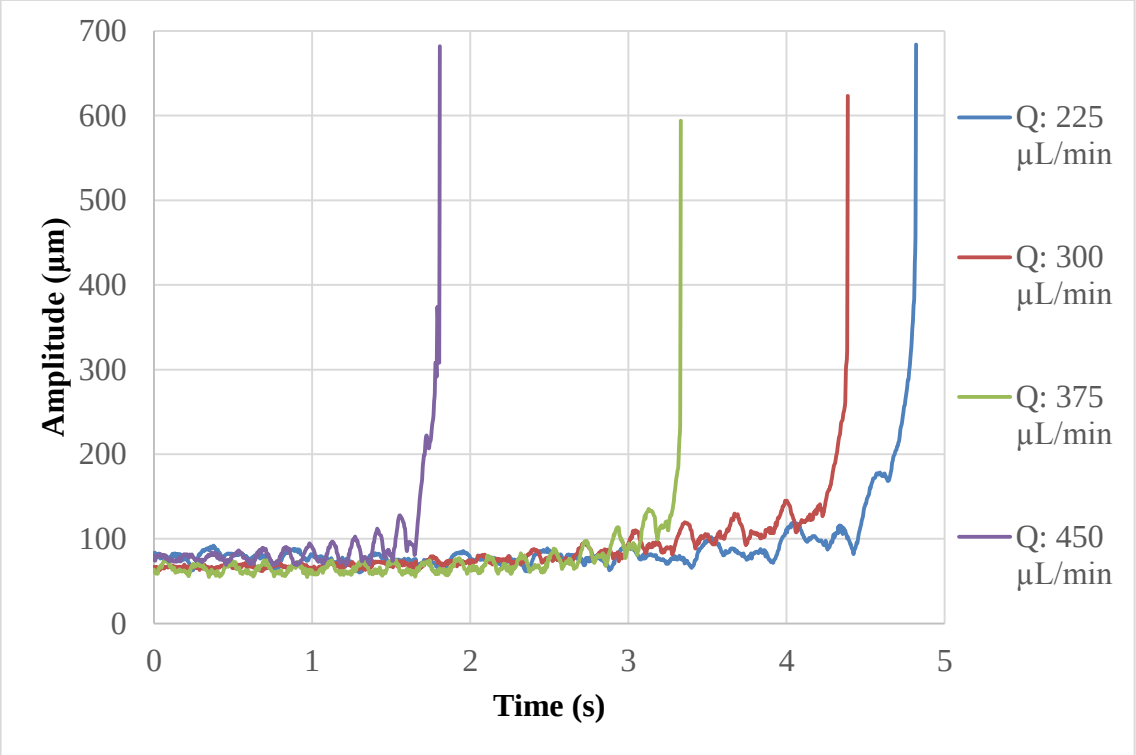

Figure 4.11. The effect of Q on the elapsed time for the first hit.

In the next sections, the effect of the applied voltage on the size of the droplets is investigated for three parameters, which are μ_r, Q_r and Q and finally an empirical model for the droplet size is established. While investigating the effect of the voltage, the experiments were performed at a range of voltage between 650 and 1850 V. For each experiment three or four different voltage value from that range, were applied. The lowest of these voltage values were chosen as to be slightly higher than the critical voltage in order to destabilize

the interface and eventually to form droplets. The other voltage values were chosen as to be 200 V higher than the lowest one. For example, for a single experiment if the critical voltage was around 580 V, the voltages were chosen as 650, 850, 1050 and 1250V. Since the critical voltage values were already known (given in Section 4.2), the voltage values to be applied were decided before performing the experiment. During the experiments, while tuning the voltage value, the voltages were arranged by starting from 0V to the desired value. When the voltage reached its critical value, the interface was ruptured and the droplets started to be formed (see Section 4.2). Therefore, the first droplets were formed in the channel at a voltage which was not the desired value for the droplet size measurements. However, the droplet sizes were changing while increasing the voltage. The sizes were decreasing with an increase in voltage and the sizes of the droplets were increasing back with a decrease in the voltage. It means that the droplets were responding to the change in voltage. The measurements were made when the voltage was tuned to the desired value. When the desired voltage value was reached, around 10s was waited to record the videos of droplets. The reason behind that was to make correct measurement waiting the lapse of response time of the droplets to the change in voltage. In the droplet size calculation, the average of at least three droplets was taken and the experiments were repeated at least three times.

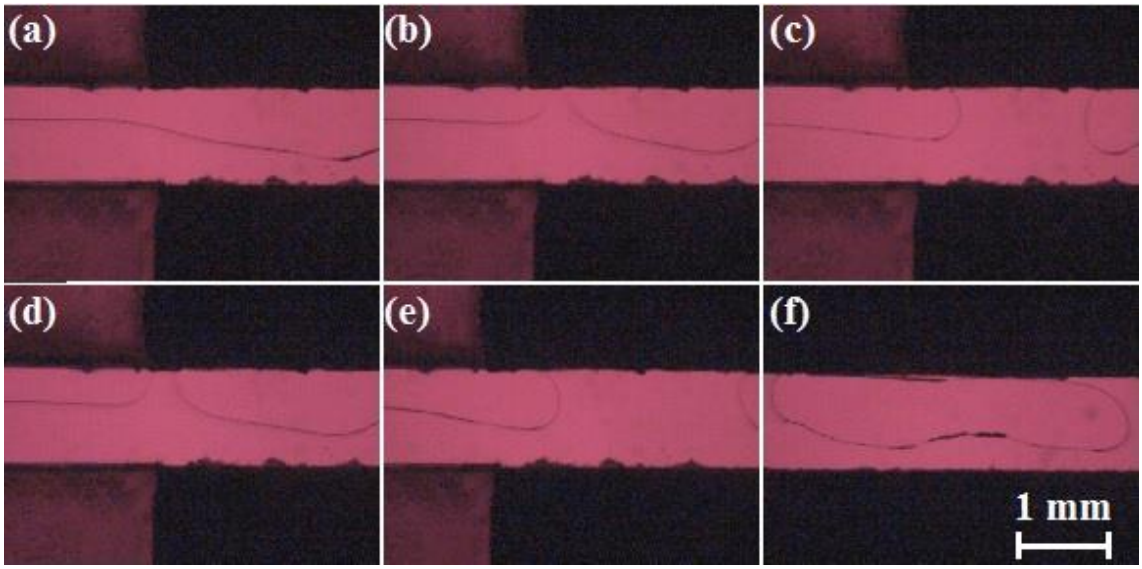

Figure 4.12. The droplet formation mechanism under normal electric field. The critical V is 630V. $Q^{(1)}$: 100μL/min, $Q^{(2)}$: 200μL/min and μr: 2.929.

4.4.1. The Effect of Voltage at Different Viscosity Ratios

In this section, the effect of the voltage on the size of the droplets which are formed due to the instability of the interface is examined for various μ_r. Other parameters such as the depth ratio H_r and the total flow rate Q are fixed. Only the Q_r is set to different values at each value of μ_r in order to set H_r to a constant specific value of 0.789 for each experiment. The reason behind this adjustment of Q_r is that the H_r of the interface changes due to the change in μ_r of the liquid couple at constant Q_r.

In these experiments, ethylene glycol and various viscosity silicone oils are used. Since the total flow rate Q is fixed at 300 μL/min, $Q^{(1)}$ and $Q^{(2)}$ were arranged to 135 and 165 μL/min for the experiments at μ_r of 0.556, to 120 and 180 μL/min for the experiments at μ_r of 1.183, to 100 and 200 μL/min for experiments at μ_r of 2.929 and to 80 and 220 μL/min for the experiments at μ_r of 5.886. It means that Q_r is not fixed at a specific value but the corresponding H_r is tried to be set at 0.789 for the experiments. In order to determine the Q_r corresponding to the desired H_r, a computer code in MATLAB, was used. The Q_r and μ_r yielding Hr is given in Table 4.1.

Table 4.1. The parameters used in the experiments for observing the effect of voltage at different viscosity ratios.

Liquids	**$Q^{(1)}$ (μL/min)**	**$Q^{(2)}$ (μL/min)**	**Q_r**	**μ_r**	**H_r**	**Applied voltages (V)**
Silicone Oil (10 cSt) / Ethylene Glycol	135	165	0.818	0.556	0.788	650, 850, 1050, 1250
Silicone Oil (20 cSt) / Ethylene Glycol	120	180	0.667	1.183	0.786	650, 850, 1050, 1250
Silicone Oil (50 cSt) / Ethylene Glycol	100	200	0.5	2.929	0.791	650, 850, 1050, 1250
Silicone Oil (100 cSt) / Ethylene Glycol	80	220	0.36	5.886	0.789	850, 1050, 1250, 1450

In order to see the effect of the voltage on the droplet size at μr of 0.556, 1.183, 2.929 and 5.886, the voltage values are chosen as 650, 850, 1050 and 1250 V. All these voltages are above the critical voltage to destabilize the interface. Only for the liquid couple at μr of 5.886, 650 V is under its critical voltage. Therefore, for that experiment, 1450 V is used instead of 650 V.

The effect of the voltage on the droplet size at four different μ_r is shown in Figure 4.13. The results indicate that an increase in the voltage causes a reduction of the droplet size, which is in accordance with Ozen *et al.* (2006). Moreover, the correlation between the voltage and the droplet size shows a negative power law relation. It means that an increase of the voltage at higher voltage values, results in a less decrease in the droplet size. At a very high voltage, the droplet sizes will be very close to each other for all viscosity ratios, around 10^{-11} m^3 (10^{-2} μL). Furthermore, at the same voltage the droplet size of the less viscous liquid is larger.

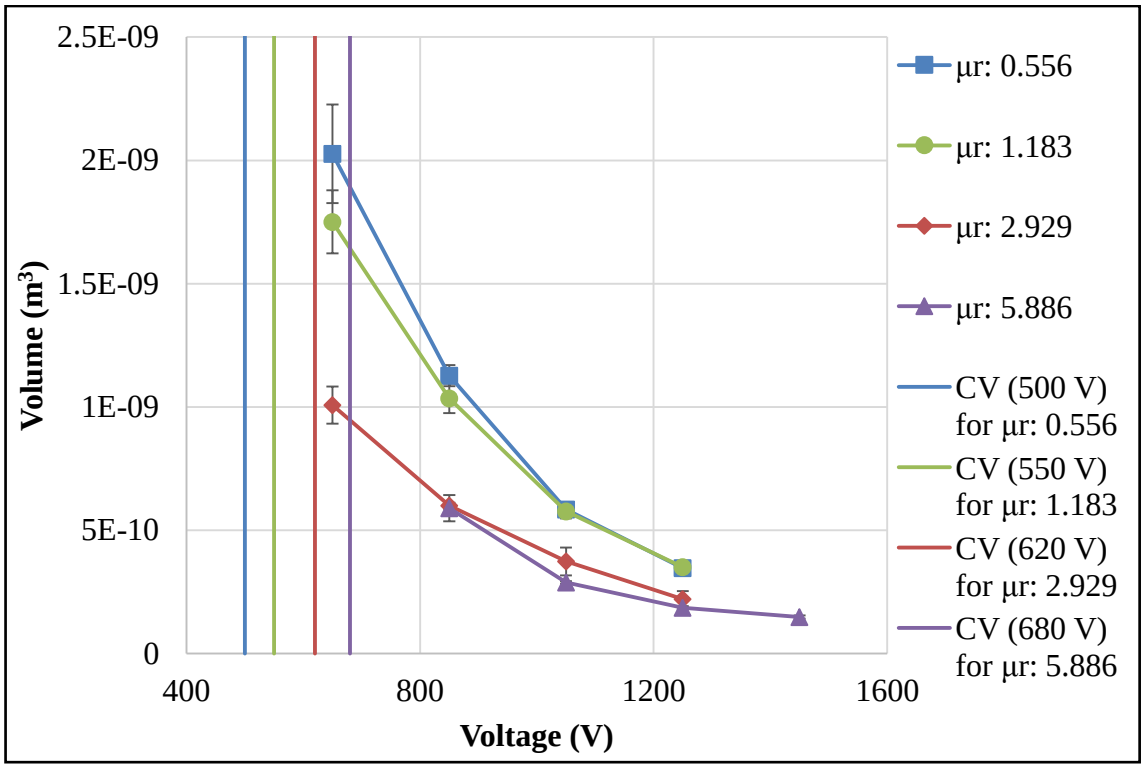

Figure 4.13. The effect of voltage on the droplet size at different μ_r.

The effect of the electric number, E_b on the droplet size is shown in Figure 4.14. As seen in Equation 4.1, the voltage is squared in E_b and E_b contains the height of the ethylene glycol, i.e. $H^{(2)}$, which is not constant as the μ_r changes. Furthermore, even though as E_b increases the droplet volume decreases, but the decrease in droplet volume might not be same or similar when V increases.

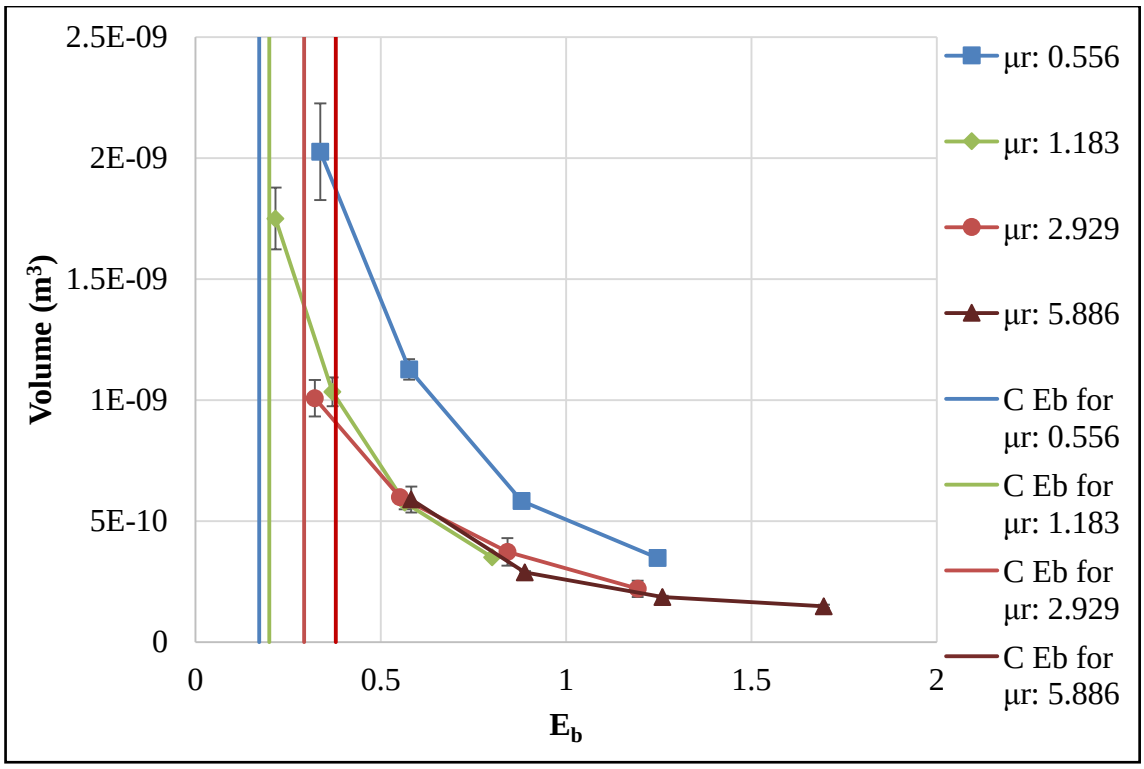

Figure 4.14. The effect of E_b on the droplet size at different μ_r.

4.4.2. The Effect of Voltage at Different Flow Rate Ratios

In this section, the effect of the voltage on the size of the droplets which are formed due to the instability of the interface is examined for various volumetric flow rate ratios Q_r.

In these experiments, ethylene glycol and 50 cSt silicone oil are used. Therefore, μ_r is set to 2.929. The total flow rate Q is also fixed at a value of 300 μL/min. In order to see the effect of the voltage on the droplet size at Q_r of 0.5, 1 and 2, the voltage values to apply are chosen from a range between 650 and 1850 V. The differences between the chosen voltage

values are based on the reason mentioned in Section 4.4. The table below shows the values of the parameters used in the experiments.

Table 4.2. The parameters used in the experiments for observing the effect of voltage at different flow rate ratios.

Liquids	**$Q^{(1)}$ (µL/min)**	**$Q^{(2)}$ (µL/min)**	**Q_r**	**μ_r**	**Applied voltages (V)**
Silicone Oil (50 cSt) / Ethylene Glycol	200	100	2	2.929	650, 850, 1050, 1250
Silicone Oil (50 cSt) / Ethylene Glycol	150	150	1	2.929	1050, 1250, 1450, 1650
Silicone Oil (50 cSt) / Ethylene Glycol	100	200	0.5	2.929	1250, 1450, 1650, 1850

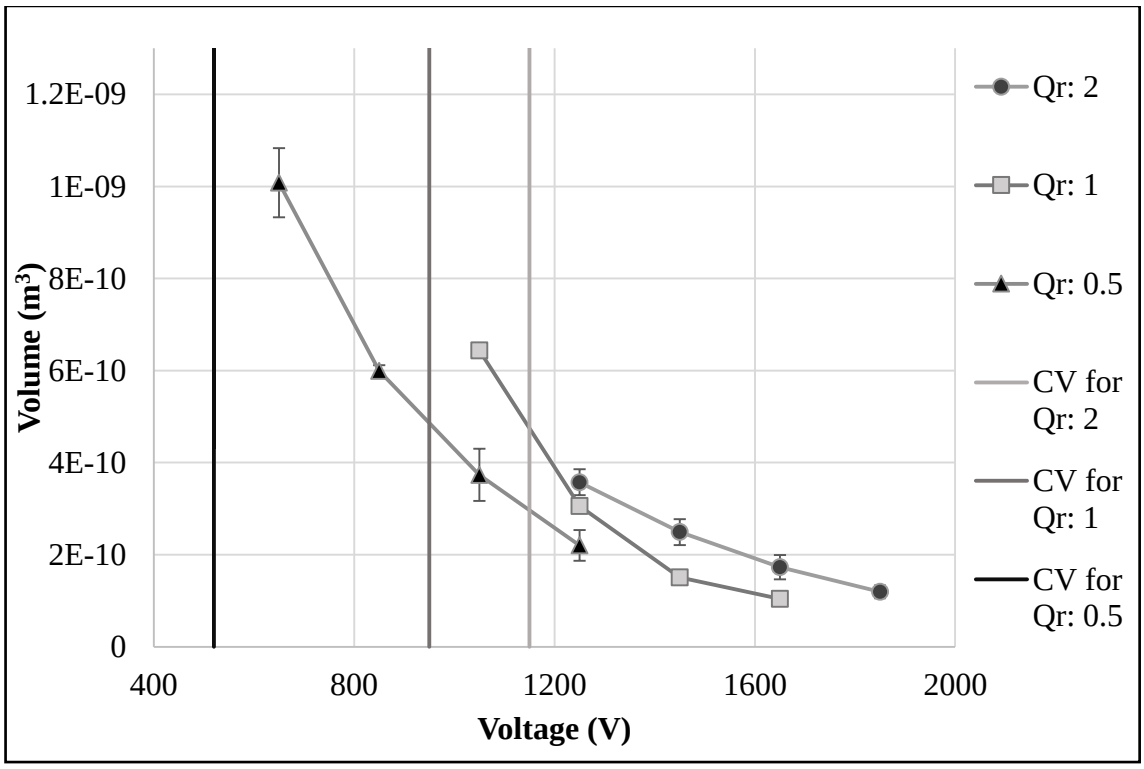

Figure 4.15. The effect of voltage on the droplet size at different Q_r.

The effect of the voltage on the droplet size at three different Q_r is shown in Figure 4.15. The results indicate that an increase in the voltage causes a reduction of the droplet size as seen in the previous section. In this investigation, at the same voltage the droplet size is larger for higher Q_r.

The effect of the electric number, E_b on the droplet size is shown in Figure 4.16. As discussed in previous section, the voltage is squared in E_b and E_b contains the height of the ethylene glycol, i.e. $H^{(2)}$, which is not constant as the Q_r changes. Consequently, even the effect of the voltage and the E_b are similar, each set of point which correspond a single Q_r, are more distant to each other in E_b figure (Figure 4.16) than that in V figure (Figure 4.15).

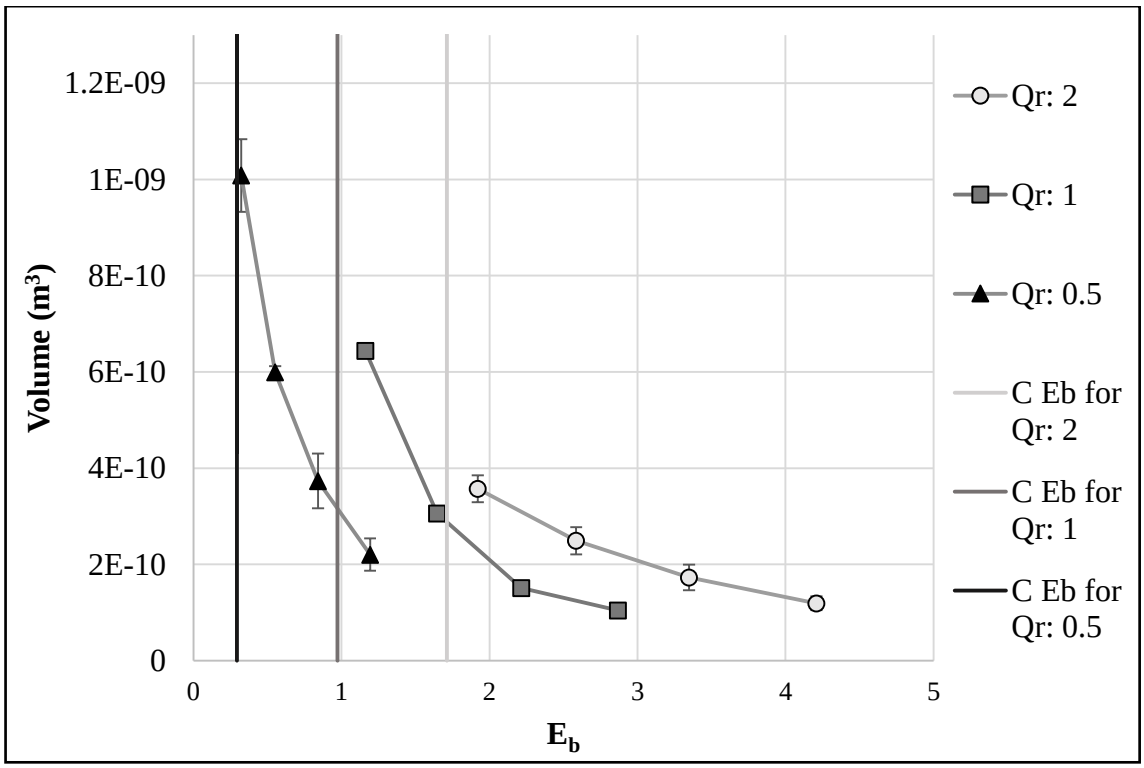

Figure 4.16. The effect of E_b on the droplet size at different Q_r.

4.4.3. The Effect of Voltage at Different Total Flow Rate

In this section, the effect of the voltage on the size of the droplets which are formed due to the instability of the interface is examined for various total flow rate Q.

In these experiments, ethylene glycol and 50 cSt silicone oil are used. Therefore, μ_r is set to 2.929. The volumetric flow rate ratio Q_r is fixed at 0.5. In order to see the effect of the voltage on the droplet size at four different total flow rates, Q is chosen as 225, 300, 375 and 450 μL/min, the voltage values to apply are chosen 650, 850, 1050 and 1250 V for all Qs. The table below shows the values of the parameters used in the experiments.

Table 4.3. The parameters used in the experiments for observing the effect of voltage at different total flow rates.

Liquids	**$Q^{(1)}$ (μL/min)**	**$Q^{(2)}$ (μL/min)**	**Q (μL/min)**	**μ_r**	**Applied voltages (V)**
Silicone Oil (50 cSt) / Ethylene Glycol	75	150	225	2.929	650, 850, 1050, 1250
Silicone Oil (50 cSt) / Ethylene Glycol	100	200	300	2.929	650, 850, 1050, 1250
Silicone Oil (50 cSt) / Ethylene Glycol	125	250	375	2.929	650, 850, 1050, 1250
Silicone Oil (50 cSt) / Ethylene Glycol	150	300	450	2.929	650, 850, 1050, 1250

The effect of the voltage on the droplet size at four different total flow rates, Q is shown in Figure 4.17. When Q increases, the size of the droplets decreases. The effect of the electric number, E_b on the droplet size is also shown in Figure 4.18. The trends are very similar in both figures. The difference comes from that the voltage is squared in E_b (Equation 4.1). Moreover, the depth of the ethylene glycol, $H^{(2)}$ which is present in Equation 4.1 is not exactly same for each experiment. Even the flow rate ratios, Q_r are same for these set of experiments, due to the experimental errors, small differences occur in depth ratio. Therefore, when the droplet sizes at same V, but at different Q is comparable, they are not comparable at the same E_b. The effect of the total flow rate on the droplet size may be also compared with the results obtained in Figure 4.11. As mentioned in Section 4.3, when the total flow rate Q is increased the interface hits the wall faster. This increases the frequency of the droplet formation, resulting in smaller droplets (Figure. 4.17). Therefore, since the faster hits results in smaller droplets, the observations accord with the results in Section 4.3.

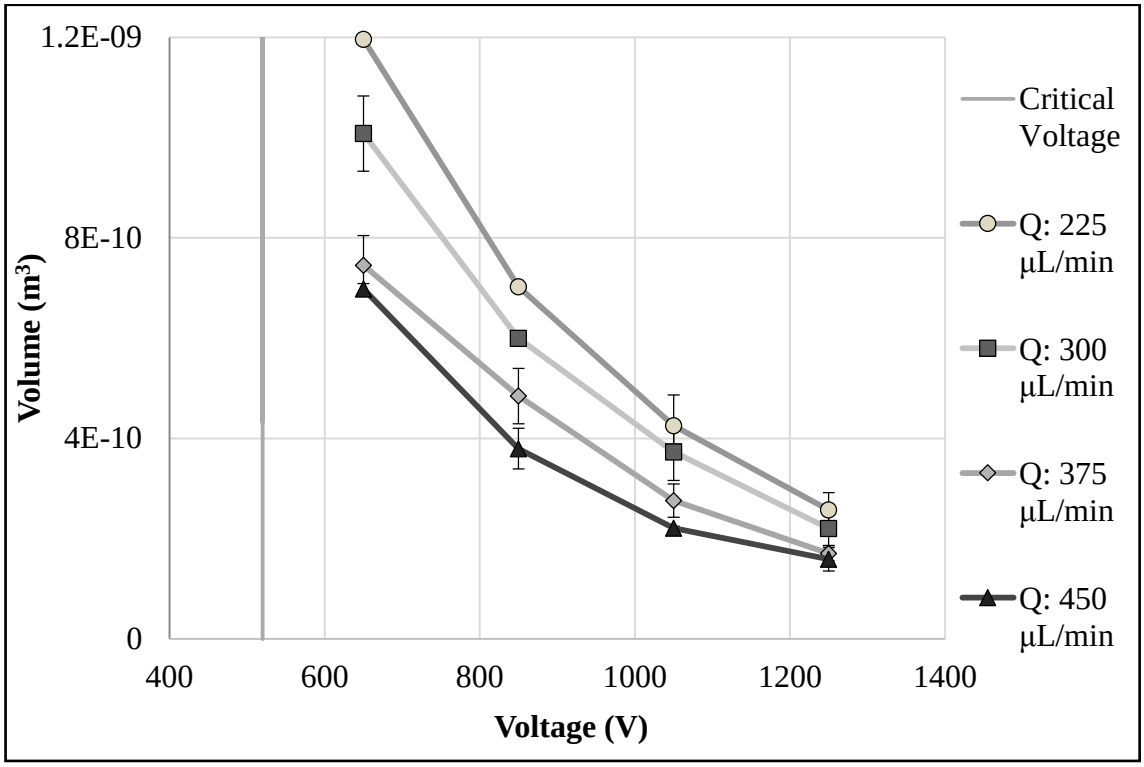

Figure 4.17. The effect of voltage on the droplet size at different Q.

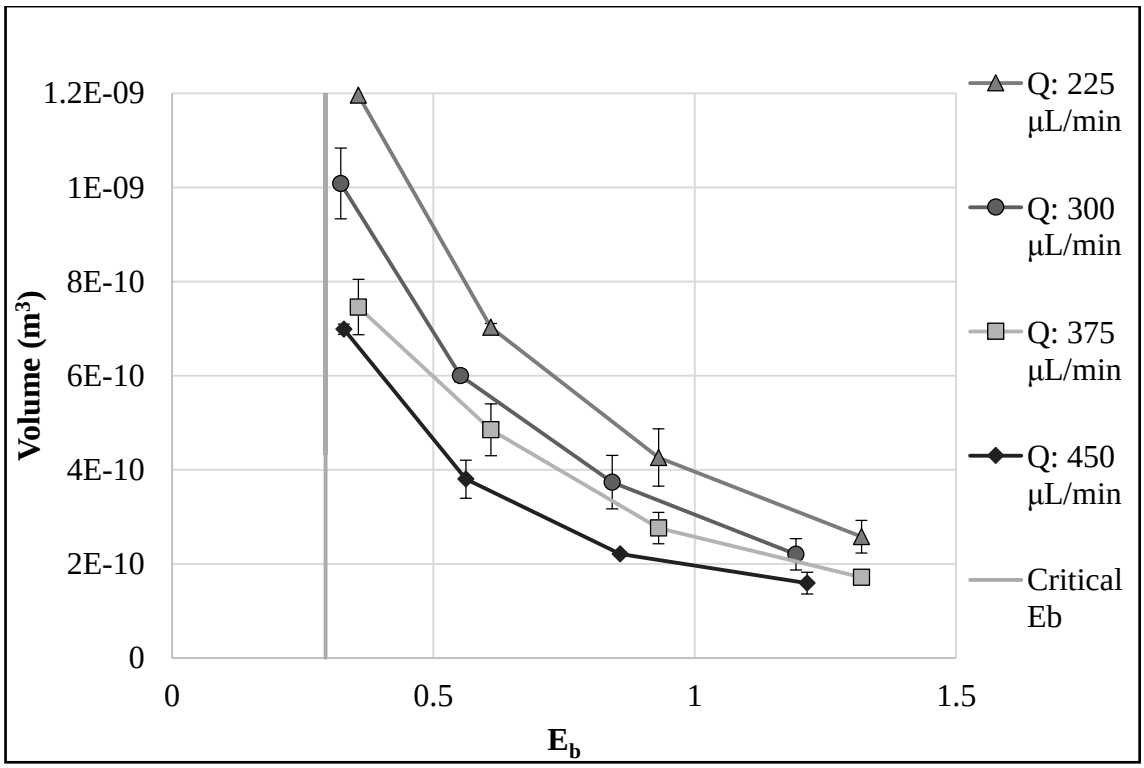

Figure 4.18. The effect of E_b on the droplet size at different Q.

4.4.4. Empirical Model for Droplet Size

In this section, the results in terms of the droplet size obtained from each experiment is expressed as a function of the parameters which are E_b, Q, H_r and μ_r. In this model H_r is used instead of Q_r due to the same reasons explained in Section 4.2.4. Therefore, in our model H_r, which is measured for each experiment is used for defining the model for the droplet size. Apart from the droplet size model at the several voltage values and the several corresponding E_b, a droplet size model at the critical voltage is also proposed. That model is established by combining the critical E_b model which is determined in Section 4.2.4 and the droplet size model (Equation 4.3).

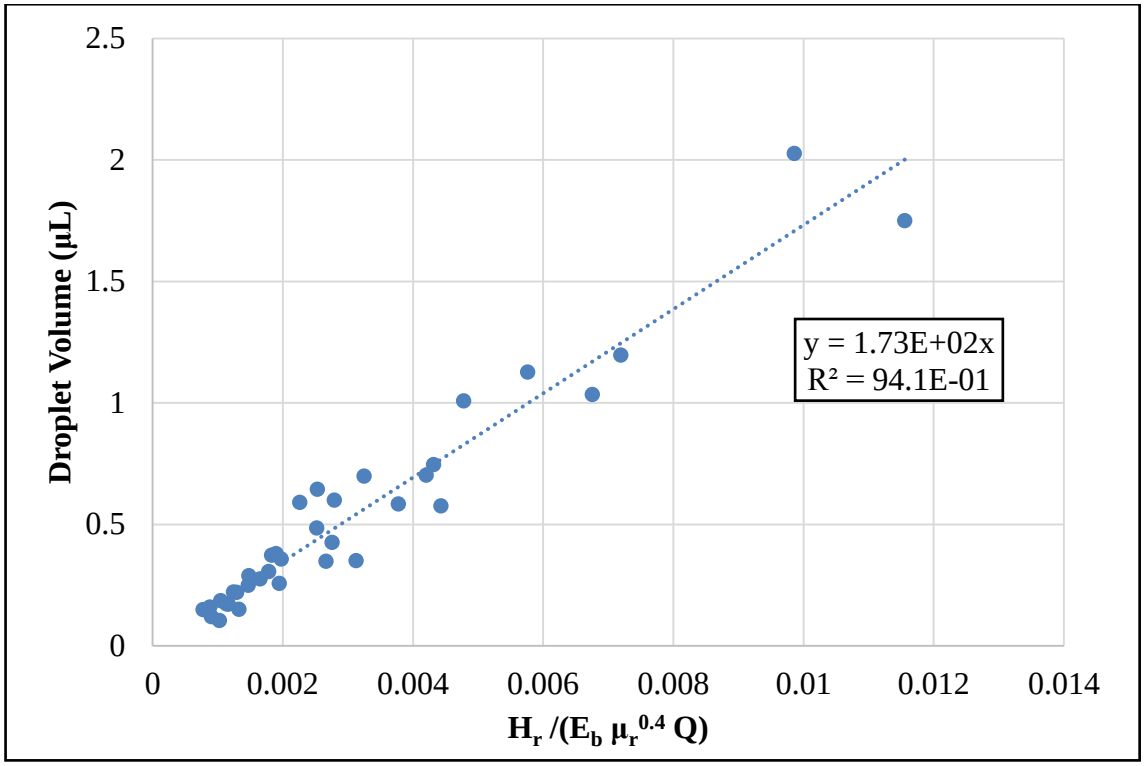

Figure 4.19. The linear fitting for the empirical model of droplet volume as a function of E_b, H_r, μ_r and Q (given in µL/min).

The experiments are carried out at different voltages which are in the range between 650V and 1850V for μ_r of 0.556, 1.183, 2.929 and 5.886, for several H_r (as a result of Q_r) and for Q of 225, 300, 375 and 450 µL/min.

Figure 4.19 shows the linear fitting of the model. The factors and the coefficients of the model were determined by using polyfit function in MATLAB. The droplet volume is a function of μ_r with a power of (-0.4), H_r with a power of 1, E_b with a power of (-1) and Q with a power (-1). Therefore, the empirical model can be expressed as below.

$$\text{Droplet Volume} = \frac{173\ x\ H_r}{E_b\ {\mu_r}^{0.4}\ Q} \tag{4.3}$$

where the unit of the total flow rate, Q is μL/min and the droplet volumes are in μL.

The empirical equation shows that the H_r has a positive effect on the determination of the droplet volume while the μ_r has a negative effect.

A model derived for critical E_b as a function of H_r and μ_r. Therefore, at the critical E_b which is a function of critical voltage, the droplet sizes can be expressed only with H_r, μ_r and Q by combining both models.

$$\text{Droplet Volume at Critical } V = \frac{467}{{H_r}^{0.67}\ {\mu_r}^{0.65}\ Q} \tag{4.4}$$

where the unit of the total flow rate, Q is μL/min and the droplet volumes are in μL.

According to the model, the effect of the H_r and the μ_r on the droplet size is comparable to each other at the critical voltage. H_r has a negative effect unlike in Equation 4.3.

5. CONCLUSIONS AND RECOMMENDATIONS

5.1. Conclusions

The electrodynamic instability of the interface between two immiscible Newtonian liquids is studied experimentally in three parts. Firstly, the deflection of the interface at a critical voltage value is investigated, secondly the nonlinear evolution of the interface is examined and finally the droplet formation mechanism is analyzed.

In the first part, the critical voltage value at which the first deflection of the interface occurs is determined for three parameters which are the viscosity ratio, the flow rate ratio and the total flow rate. As a result, it is observed that an increase in the viscosity ratio or the flow rate ratio shows a stabilizing effect of the interface and it results in an increase of the critical voltage value. Furthermore, it is observed that the total flow rate has no effect on the critical voltage. Based on the results obtained from the experiments, an empirical model is established. According to that model, the dimensionless electric number is found as a function of the depth ratio with a power of 1.67 and the viscosity ratio with a power of 0.25. By comparing the factors, it can be said that the depth ratio has an effect more dominant than that of viscosity ratio on the critical electric number.

In the second part, the elapsed time between the first deflection and the rupture of the interface is determined for different total flow rates. Moreover, the time dependent positional change of the maximum point at the interface is analyzed. As a result, it is observed that an increase in the total flow rate at the same voltage results in shortening of the elapsed time for the rupture of the interface. That observation may also be interpreted as an explanation for the correlation between the droplet size and the total flow rate. A decrease in the time for the interface to hit the wall increases the frequency of the hit. Therefore, the area of the interface between the two points at which the interface is ruptured becomes smaller. Since the droplets are formed based on the coalescence of these two points, the area of the interface between those two points becomes the surface area of the droplet. The elapsed time for interface to hit periodically the wall can correlated to the droplet size. Therefore, a shortening in the elapsed time may result in a decrease in the size of the droplets.

In the third part, the sizes of the droplets are determined at various voltage values for the same three parameters, i.e. the viscosity ratio, the flow rate ratio and the total flow rate. According to the results, for all parameters an increase in the voltage ends up with smaller droplets. Moreover, at higher viscosity ratio, lower flow rate ratio or higher total flow rate the droplet sizes become smaller. These correlations are also seen in the model expressed in Equation 4.3. Based on the results obtained from the experiments, an empirical model is established. According to that model, the droplet size is found as a function of the depth ratio with a power of -1 and the viscosity ratio with a power of -0.4. By comparing the factors, it can be said that the depth ratio has an effect more dominant than that of the viscosity ratio on the droplet size. However, at the critical voltage, the viscosity ratio and the depth ratio have similar.

5.2. Recommendations

In determining the critical voltage and the droplet formation parts, three parameters which are the flow rate ratio, the viscosity ratio and the total flow rate are used. According to the results obtained from the experiments, two empirical models are established based on these parameters. Although the models are very suitable for the liquid couples and the microchannel with specific dimensions, the model can serve for a wider application area by including more parameters. Apart from these three parameters, the width of the channel can also be used. Moreover, the electrical conductivity ratio and the permittivity ratio can be considered in the case of performing experiments with different liquid couples.

The applied electric field is normal to the flow direction in all cases. The work is limited with the normal electric field. However, the effect of the direction of the electric field can be investigated by using an electric field parallel to the flow direction.

The droplets are formed as silicone oil droplets for all experiments. The reason behind this fact can be investigated. It means that the responsible parameter can be found by using different liquid couples.

In the nonlinear analysis part, the only parameter used is the total flow rate. The other parameters are still pending to make better expression on the nonlinear evolution of the interface. Moreover, these results can be checked with the numerical models in the literature. The wavelength of the destabilized interface under the effect of an electric field or the growth rate of the destabilization until its rupture can be compared.

REFERENCES

Abdella, K., H. Rasmussen, and I. I. Inculet, 1996, "Interfacial Deformation of Liquid Drops by Electric Fields at Zero Gravity", *Computers & Mathematics with Applications*, Vol. 31, No. 10, pp. 67–82.

Abe, K., K. Suzuki, and D. Citterio, 2008, "Inkjet-Printed Microfluidic Multianalyte Chemical Sensing Paper", *Analytical Chemistry*, Vol. 80, No. 18, pp. 6928–6934.

Anna, S. L., N. Bontoux, and H. A. Stone, 2003, "Formation of Dispersions Using 'Flow Focusing' in Microchannels", *Applied Physics Letters*, Vol. 82, No. 3, pp. 364–366.

Atalay, Y. T., S. Vermeir, D. Witters, N. Vergauwe, B. Verbruggen, P. Verboven, B. M. Nicolaï and J. Lammertyn, 2011, "Microfluidic Analytical Aystems for Food Analysis", *Trends in Food Science & Technology*, Vol. 22, No. 7, pp. 386–404.

Atencia, J. and D. J. Beebe, 2005, "Controlled Microfluidic Interfaces", *Nature*, Vol. 437, No. 7059, pp. 648–655.

Avsec, D. and M. Luntz, 1936, "Tourbillons Electroconvectifs," *Comptes Rendus de l'Académie des Sciences*, Vol. 203, pp. 1140–1144.

Bandyopadhyay, D., A. Sharma, U. Thiele, P. Dinesh, and S. Reddy, 2009, "Electric-Field-Induced Interfacial Instabilities and Morphologies of Thin Viscous and Elastic Bilayers", *Langmuir*, Vol. 25, No. 16, pp. 9108–9118.

Becker, H. and L. E. Locascio, 2002, "Polymer Microfluidic Devices", *Talanta*, Vol. 56, No. 2, pp. 267–287.

Bulutoglu, P. S., S. Koc, and A. K. Avci, 2016, "Simulation of Exhaust Gas Reforming of Natural Gas in a Microchannel Reactor", *International Journal of Hydrogen Energy*, Vol. 41, No. 19, pp. 8184–8192.

Casadevall Solvas, X. and A. deMello, 2011, "Droplet Microfluidics: Recent Developments and Future Applications", *Chemical Communications*, Vol. 47, pp. 1936–1942.

Castellanos, A., *Electrohydrodynamics*, Springer, 1998.

Castellanos A. and A. Gonzalez, 1998, "Nonlinear Electrohydrodynamics of Free Surfaces", *IEEE Transactions on Dielectrics and Electrical Insulation*, Vol. 5, No. 3, pp. 334–343.

Chen, C.-H., H. Lin, S. K. Lele, and J. G. Santiago, "Electrokinetic Microflow Instability with Conductivity Gradients", in *7th International Conference on Miniaturized Chemical and Biological Analysis Systems*, 2003, pp. 983–987.

Chen C.-H., "Electrohydrodynamic Stability", in *Electrokinetics and Electrohydrodynamics in Microsystems*, Vienna, 2011, pp. 177–220.

Chiu, D. T., E. Pezzoli, H. Wu, A. D. Stroock, and G. M. Whitesides, 2011, "Using Three-Dimensional Microfluidic Networks for Solving Computationally Hard Problems", *Proceedings of the National Academy of Sciences of the United States of America*, Vol. 98, No. 6, pp. 2961-2966.

Craster, R. V. and K. Matar, 2005, "Electrically Induced Pattern Formation in Thin Leaky Dielectric Films", *Physics of Fluids*, Vol. 17.

de Mello, A. J., 2011 "Focus", *Lab on a Chip*, Vol. 1, No. 2, p. 24N.

El Moctar, A. O., N. Aubry, and J. Batton, 2003, "Electro-Hydrodynamic Micro-Fluidic Mixer", *Lab on a Chip*, Vol. 3, No. 4, pp. 273.

Eow, J. S. and M. Ghadiri, 2003, "The Behaviour of a Liquid–Liquid Interface and Drop-Interface Coalescence under the Influence of an Electric Field", *Colloids and Surfaces A: Physicochemical and Engineering Aspects*, Vol. 215, No. 1, pp. 101–123.

Eribol, P. and A. K. Uguz, 2015, “Experimental Investigation of Electrohydrodynamic Instabilities in Micro Channels”, *European Physical Journal Special Topics*, Vol. 224, pp. 425–434.

Ersoy, G. and A. Kerem Uguz, 2012, “Electro-Hydrodynamic Instability in a Microchannel between a Newtonian and a Non-Newtonian Liquid”, *Fluid Dynamics Research*, Vol. 44, No. 3, pp. 031406.

Fenton, E. M., M. R. Mascarenas, G. P. López, and S. S. Sibbett, 2009, “Multiplex Lateral-Flow Test Strips Fabricated by Two-Dimensional Shaping”, *ACS Applied Materials & Interfaces*, Vol. 1, No. 1, pp. 124–129.

Fiorini G. S., G. D. M. Jeffries, 2003, D. S. W. Lim, C. L. Kuyper, and D. T. Chiu, “Fabrication of Thermoset Polyester Microfluidic Devices and Embossing Masters Using Rapid Prototyped Polydimethylsiloxane Molds”, *Lab on a Chip*, Vol. 3, No. 3, pp. 158.

Fiorini, G. S., R. M. Lorenz, and J. S. Kuo, and D. T. Chiu, 2004, “Rapid Prototyping of Thermoset Polyester Microfluidic Devices”, *Analytical Chemistry*, Vol. 76, No.16, pp. 4697-4704.

Fiorini, G. S. and D. T. Chiu, 2005, “Disposable Microfluidic Devices: Fabrication, Function, and Application.”, *BioTechniques*, Vol. 38, No. 3, pp. 429–46.

Fong L. K., 2015, "Materials and Fabrication Techniques for Nano-and Microfluidic Devices", *Royal Society of Chemistry*, pp. 28.

Fujino, T., Y. Yokoyama, and Y. H. Mori, 1989, “Augmentation of Laminar Forced-Convective Heat Transfer by the Application of a Transverse Electric Field”, *Journal of Heat Transfer*, Vol. 111, No. 2, pp. 345.

Gambhire, P. and R. M. Thaokar, 2010, “Electrohydrodynamic Instabilities at Interfaces Subjected to Alternating Electric Field”, *Physics of Fluids*, Vol. 22.

Gañán-Calvo, A. M., 1998, "Generation of Steady Liquid Microthreads and Micron-Sized Monodisperse Sprays in Gas Streams", *Physical Review Letters*, Vol. 80, No. 2, pp. 285–288.

Gemant, A., 1929, "Electrotech", *Zeit*, Vol. 34, pp. 1225.

Gilbert, W., *De Magnete*. Chiswick Press, 1600.

Gu, H., M. H. G. Duits and F. Mugele, 2011, "Droplets Formation and Merging in Two-Phase Flow Microfluidics", *International journal of molecular sciences*, Vol. 12, No. 4, pp. 2572–2597.

Ha, J.-W. and S.-M. Yang, 2000, "Deformation and Breakup of Newtonian and Non-Newtonian Conducting Drops in an Electric Field", *Journal of Fluid Mechanics*, Vol. 405, pp. 131-156.

Hatakeyama, T., Delai L. Chen, and R. F. Ismagilov, 2006, "Microgram-Scale Testing of Reaction Conditions in Solution Using Nanoliter Plugs in Microfluidics with Detection by MALDI-MS", *Journal of the American Chemical Society*, Vol. 128, No. 8, pp. 2518-2519.

Hoburg, J. F. and J. R. Melcher, 1976, "Internal Electrohydrodynamic Instability and Mixing of Fluids with Orthogonal Field and Conductivity Gradients", *Journal of Fluid Mechanics*, Vol. 73, No. 02, pp. 333.

Hosokawa, K., T. Fujii, and I. Endo, 1999, "Droplet-Based Nano/Picoliter Mixer Using Hydrophobic Microcapillary Vent", in *Technical Digest. IEEE International MEMS 99 Conference. Twelfth IEEE International Conference on Micro Electro Mechanical Systems (Cat. No.99CH36291)*, pp. 388–393.

Hsiao, A. Y., 2009, "Microfluidic System for Formation Of PC-3 Prostate Cancer Co-Culture Spheroids", *Biomaterials*, Vol. 30, No. 16, pp. 3020–3027.

Jeon, J. S., S. Chung, R. D. Kamm, and J. L. Charest, 2011, "Hot Embossing for Fabrication of a Microfluidic 3D Cell Culture Platform", *Biomedical Microdevices*, Vol. 13, No. 2, pp. 325–333.

Jun Kang, Y., J. Ryu, and S.-J. Lee, 2013, "Label-Free Viscosity Measurement Of Complex Fluids Using Reversal Flow Switching Manipulation In A Microfluidic Channel", *Biomicrofluidics*, Vol. 7, No. 4, pp. 044106.

Kamholz, A. E., B. H. Weigl, B. A. Finlayson, and P. Yager, 1999, "Quantitative Analysis of molecular Interaction in a Microfluidic Channel: the T-sensor.", *Analytical Chemistry*, Vol. 71, No. 23, pp. 5340–7.

Khorshidi, B., M. Jalaal, E. Esmaeilzadeh, and F. Mohammadi, 2010, "Characteristics of Deformation and Electrical Charging of Large Water Drops Immersed in an Insulating Liquid on the Electrode Surface", *Journal of Colloid and Interface Science*, Vol. 352, No. 1, pp. 211–220.

Khorshidi, B., M. Jalaal, and E. Esmaeilzadeh, 2010, "Electrohydrodynamic Instability at the Interface Between Two Leaky Dielectric Fluid Layers", *Journal of Colloid and Interface Science*, Vol. 352, No. 1, pp. 211–220.

Lacroix, J. C., P. Atten, and E. J. Hopfinger, 1975, "Electro-Convection In A Dielectric Liquid Layer Subjected To Unipolar Injection", *Journal of Fluid Mechanics*, Vol. 69, No. 03, pp. 539.

Lagally, E. T., P. C. Simpson, and R. A. Mathies, 2000, "Monolithic Integrated Microfluidic DNA Amplification and Capillary Electrophoresis Analysis System", *Sensors and Actuators B: Chemical*, Vol. 63, No. 3, pp. 138–146.

Li, F., O. Ozen, N. Aubry, D. T. Papageorgiou, and P. G. Petropoulos, 2007, "Linear Stability of a Two-Fluid Interface for Electrohydrodynamic Mixing in a Channel", *Journal of Fluid Mechanics*, Vol. 583, pp. 347.

Lin, Z., T. Kerle, T. P. Russell, E. Scha, and U. Steiner, 2002, "Structure Formation at the Interface of Liquid/Liquid Bilayer in Electric Field", *Macromolecules*, Vol. 35, pp. 3971–3976.

Lu, R., W. Shi, L. Jiang, J. Qin, and B. Lin, 2009, "Rapid Prototyping of Paper-Based Microfluidics with Wax for Low-Cost, Portable Bioassay", *Electrophoresis*, Vol. 30, No. 9, pp. 1497-1500.

Magnusson, E. B., S. Halldorsson, R. M. T. Fleming, and K. Leosson, 2013, "Real-Time Optical Ph Measurement in a Standard Microfluidic Cell Culture System", *Biomedical optics express*, Vol. 4, No. 9, pp. 1749–58.

Martinez, A. W., S. T. Phillips, M. J. Butte, and G. M. Whitesides, 2007, "Patterned Paper as a Platform for Inexpensive, Low-Volume, Portable Bioassays", *Angewandte Chemie International Edition*, Vol. 46, No. 8, pp. 1318–1320.

Martynova, L., L. E. Locascio, M. Gaitan, G. W. Kramer, and R. G. Christensen, and W. A. MacCrehan, 1997, "Fabrication of Plastic Microfluid Channels by Imprinting Methods", *Analytical Chemistry*, Vol. 69, No. 23, pp. 4783-4789.

McCormick, R. M., R. J. Nelson, M. G. Alonso-Amigo, D. J. Benvegnu, and H. H. Hooper, 1997, "Microchannel Electrophoretic Separations of DNA in Injection-Molded Plastic Substrates", *Analytical Chemistry*, Vol. 69, No. 14, pp. 2626-2630.

McDonald, J. C. and G. M. Whitesides, 2000, "Fabrication of Microfluidic Systems in Poly(dimethylsiloxane)", *Electrophoresis*, Vol. 21, no. 1, pp. 27–40.

Melcher, J. R. and W. J. Schwarz, 1968, "Interfacial Relaxation Overstability in a Tangential Electric Field", *The Physics of Fluids*, Vol. 11, No. 10, pp. 2604–1348.

Melcher, J. R. and G. I. Taylor, 1969, "Electrohydrodynamics: A Review of the Role of Interfacial Shear Stresses", *Annual Review of Fluid Mechanics*, Vol. 1, No. 1, pp. 111–146.

Misra, D., 2011, “Evolution of Dielectric Science and Technology for Nanoelectronics”, *Interface magazine*, Vol. 20, No. 4, pp. 31.

Nguyen, N.-T., T.-H. Ting, Y.-F. Yap, T.-N. Wong, J. C.-K. Chai, W.-L. Ong, J. Zhou, S. Tan, and L. Yobas, 2007, “Thermally Mediated Droplet Formation in Microchannels”, *Applied Physics Letters*, Vol. 91, No. 8, pp. 084102.

Nisisako, T., T. Torii, and T. Higuchi, 2002, “Droplet Formation in a Microchannel Network”, *Lab on a Chip*, Vol. 2, No. 1, pp. 24-26.

Nunes, J. K., S. S. H. Tsai, J. Wan, and H. A. Stone, 2013, “Dripping and Jetting in Microfluidic Multiphase Flows Applied to Particle and Fibre Synthesis”, *Journal of Physics D: Applied Physics*, Vol. 46, No. 11, pp. 114002.

Nurocak, A. and A. K. Uguz, 2013, “Effect of the Direction of the Electric Field on the Interfacial Instability between a Passive Fluid and a Viscoelastic Polymer”, *The European Physical Journal Special Topics*, Vol. 219, No. 1, pp. 99–110.

Oddy, M. H., J. G. Santiago, and J. C. Mikkelsen, 2001, “Electrokinetic Instability Micromixing”, *American Chemical Society*, Vol. 73, No. 24, pp. 5822–5832.

Okushima, S., T. Nisisako, T. Torii, and T. Higuchi, 2004, “Controlled Production of Monodisperse Double Emulsions by Two-Step Droplet Breakup in Microfluidic Devices”, *Langmuir*, Vol. 20, No. 23, pp. 9905–9908.

Ozen, O., N. Aubry, D. T. Papageorgiou, and P. G. Petropoulos, 2006, “Monodisperse Drop Formation in Square Microchannels”, *Physical Review Letters*, Vol. 96, No. 14, pp. 144501.

Paillat, T. and G. Touchard, 2009, “Electrical Charges and Liquids Motion”, *Journal of Electrostatics*, Vol. 67, No. 2–3, pp. 326–334.

Ren, K., J. Zhou, and H. Wu, 2013, "Materials for Microfluidic Chip Fabrication", *Accounts of Chemical Research*, Vol. 46, No. 11, pp. 2396–2406.

Roberts, S. A. and S. Kumar, 2010, "Electrohydrodynamic Instabilities in Thin Liquid Trilayer Films", *Physics of Fluids*, Vol. 22, No. 12, pp. 122102.

Rodriguez, I., P. Spicar-Mihalic, C. L. Kuyper, G. S. Fiorini, and D. T. Chiu, 2003, "Rapid Prototyping of Glass Microchannels", *Analytica Chimica Acta*, Vol. 496, No. 1–2, pp. 205–215.

Saville, D. A., 1997, "Electrohydrodynamics: The Taylor-Melcher Leaky Dielectric Model", *Annual Review of Fluid Mechanics*, Vol. 29, No. 1, pp. 27–64.

Schwesinger, N., T. Frank, and H. Wurmus, 1996, "A Modular Microfluid System with an Integrated Micromixer", *Journal of Micromechanics and Microengineering*, Vol. 6, No. 1, pp. 99–102.

Seo, T. Y., 2012, "Immobilized Cell Microchannel Bioreactor for Evaluating Fermentation Characteristics of Mixed Substrate Consumption and Product Formation", *Process Biochemistry*, Vol. 47, No. 6, pp. 1011-1015.

Shankar, V. and A. Sharma, 2004, "Instability of the Interface between Thin Fluid Films Subjected to Electric Fields", *Journal of Colloid and Interface Science*, Vol. 274, pp. 294–308.

Slapar, V., "Microdluidics", 2008.

Song, H., D. L. Chen, and R. F. Ismagilov, 2006, "Reactions in Droplets in Microfluidic Channels", *Angewandte Chemie International Edition*, Vol. 45, No. 44, pp. 7336–7356.

Tan, S.-H., N.-T. Nguyen, L. Yobas, and T. G. Kang, 2010, "Formation and Manipulation of Ferrofluid Droplets at a Microfluidic T-Junction", *Journal of Micromechanics and Microengineering*, Vol. 20, No. 4, pp. 045004.

Taylor, G. I. and A. D. McEwan, 1965, "The Stability of a Horizontal Fluid Interface in a Vertical Electric Field", *Journal of Fluid Mechanics*, Vol. 22, No. 01, pp. 1.

Teh, S.-Y., R. Lin, L. Hung and A. P. Lee, 2008, "Droplet Microfluidics", *Lab on a Chip*, Vol. 8, No. 2, pp. 198-220.

Terry, S. C., J. H. Jerman, and J. B. Angell, 1979, "A Gas Chromatographic Air Analyzer Fabricated on a Silicon Wafer", *IEEE Transactions on Electron Devices*, Vol. 26, No. 12, pp. 1880–1886.

Thaokar, R. M. and V. Kumaran, 2005, "Electrohydrodynamic Instability of the Interface Between Two Fluids Confined in a Channel", *Physics of Fluids*, Vol. 17, No. 084104.

Thorsen, T., R. W. Roberts, F. H. Arnold, and S. R. Quake, 2001, "Dynamic Pattern Formation in a Vesicle-Generating Microfluidic Device". *Physical Review Letters*, Vol. 86, No. 18, pp. 4163–4166.

Tobazeon, R., 1984, "Electrohydrodynamic Instabilities and Electroconvection in the Transient and A.C. Regime of Unipolar Injection in Insulating Liquids: A Review", *Journal of Electrostatics*, Vol. 15, No. 3, pp. 359–384.

Turnbull, R. J., 1968, "Electroconvective Instability with a Stabilizing Temperature Gradient. I. Theory", *Physics of Fluids*, Vol. 11, No. 12, pp. 2588.

Uguz, A. K., O. Ozen, and N. Aubry, 2008, "Electric Field Effect on A-a Two-Fluid Interface Instability in Channel Flow for Fast Electric Times", *Physics of Fluids*, Vol. 20, No. 3.

Virányi, Z., T. Th, and D. O. Horváth, 2004, "Lateral Instability Induced by an Inhomogeneous Electric Field", *Chemical physics letters*, Vol. 401, No. 4, pp. 575-578.

Whitesides, G. M., E. Ostuni, S. Takayama, X. Jiang, and D. E. Ingber, 2001, "Soft Lithography in Biology and Biochemistry". *Annual Review of Biomedical Engineering*, Vol. 3, No. 1, pp. 335–373.

Whitesides, G. M., 2006, "The Origins and the Future of Microfluidics", *Nature*, Vol. 442, No. 7101, pp. 368–373.

Xia, Y. and G. M. Whitesides, 1998, "Soft Lithography", *Angewandte Chemie International Edition*, Vol. 28, No. 1, pp. 153–184.

Xiang, A., 2014, "An Aptamer-based Immunoassay in Microchannels of a Portable Snalyzer for Detection of Microcystin-leucine-arginine", *Talanta*, Vol. 130, pp. 363–369.

Xu, J., L. Locascio, M. Gaitan, and C. S. Lee, 2000, "Room-Temperature Imprinting Method for Plastic Microchannel Fabrication", *Anlaytical Chemistry*, Vol. 72, No. 8, pp. 1930-1933.

Yetisen, A. K., M. S. Akram, and C. R. Lowe, 2013, "Paper-Based Microfluidic Point-Of-Care Diagnostic Devices", *Lab on a Chip*, Vol. 13, No. 12, p. 2210.

Zhou, J., A. V. Ellis, and N. H. Voelcker, 2010, "Recent Developments in PDMS Surface Modification for Microfluidic Devices", *Electrophoresis*, Vol. 31, No. 1, pp. 2–16.

APPENDIX A: DERIVATION FOR THE DEPTH RATIO

The derivation for the depth ratio as a function of the flow rate ratio is given. The laminar velocity profiles are found by simplifying the Navier-Stokes equations as

$$\mu^{(1)} \frac{d^2 V_x^{(1)}}{dz^2} = \frac{dP}{dx} \tag{A.1}$$

and

$$\mu^{(2)} \frac{d^2 V_x^{(2)}}{dz^2} = \frac{dP}{dx} \tag{A.2}$$

for both phases. Integrating these equations give the velocity profiles, $V_x^{(1)}$ and $V_x^{(2)}$ as in Equations A.3 and A.4.

$$V_x{}^{(1)} = \alpha_1 z^2 + c1_1 z + c1_2 \tag{A.3}$$

$$V_x{}^{(2)} = \alpha_2 z^2 + c2_1 z + c2_2 \tag{A.4}$$

The unknown four constants are found from the no-slip boundary conditions on the walls (located at z = 0 and z = d1 + d2) and at the interface (located at z = d2) and the continuity of the stress at the interface given as

$$V_x^{(1)}\Big|_{z=d_1+d_2} = 0 \tag{A.5}$$

$$V_x^{(2)}\Big|_{z=0} = 0 \tag{A.6}$$

$$V_x^{(1)}\Big|_{z=d_1} = V_x^{(2)}\Big|_{z=d_1} \tag{A.7}$$

and

$$\mu^{(1)} \frac{dV_x^{(1)}}{dz}\bigg|_{z=d_1} = \mu^{(2)} \frac{dV_x^{(2)}}{dz}\bigg|_{z=d_1} \tag{A.8}$$

respectively. At this point, the pressure gradient and the interface position are unknown. These can be determined by integrating the velocities over the cross sectional areas to find the volumetric flow rates, which are known in the experiments. The integrals are

$$Q^{(1)} = D \int_{d_2}^{d_1+d_2} V_x^{(1)} dz \tag{A.9}$$

$$Q^{(2)} = D \int_{0}^{d_2} V_x^{(2)} dz \tag{A.10}$$

where D is the uniform channel depth. The position of the interface is determined in Matlab as a function of viscosity and volumetric flow rate ratios.